

1 **Contrasting strategies of hydraulic control in two co-dominant temperate tree species**

2
3 Ashley M. Matheny^{1†}, Richard P. Fiorella^{2,3}, Gil Bohrer¹, Christopher J. Poulsen², Timothy H.
4 Morin¹, Alyssa Wunderlich¹, Christoph S. Vogel⁴, and Peter S. Curtis⁵

5
6 ¹Department of Civil, Environmental, and Geodetic Engineering, The Ohio State University,
7 Columbus, Ohio 43210 USA

8 ²Department of Earth and Environmental Sciences, University of Michigan, Ann Arbor,
9 Michigan 48109 USA

10 ³Department of Geology and Geophysics, University of Utah, Salt Lake City, Utah 84112 USA

11 ⁴University of Michigan Biological Station, Pellston, Michigan 49769 USA

12 ⁵Department of Evolution, Ecology, and Organismal Biology, The Ohio State University,
13 Columbus, Ohio 43210 USA

14 [†] Email: matheny.44@osu.edu, Phone: (614)292-9582, Fax: (614)292-3780

15
16
17
18
19
20

This is the author manuscript accepted for publication and has undergone full peer review but has not been through the copyediting, typesetting, pagination and proofreading process, which may lead to differences between this version and the [Version of Record](#). Please cite this article as doi: [10.1002/eco.1815](https://doi.org/10.1002/eco.1815)

21 **Abstract**

22 Biophysical controls on plant water status exist at the leaf, stem, and root levels.
23 Therefore, we pose that hydraulic strategy is a combination of traits governing water use at each
24 of these three levels. We studied sap flux, stem water storage, stomatal conductance,
25 photosynthesis, and growth of red oaks (*Q. rubra*) and red maples (*A. rubrum*). These species
26 differ in stomatal hydraulic strategy, xylem architecture, and may root at different depths. Stable
27 isotope analysis of xylem water was used to identify root-water uptake depth. Oaks were shown
28 to access a deeper water source than maples. During non-limiting soil moisture conditions,
29 transpiration was greater in maples than oaks. However, during a soil dry down, transpiration
30 and stem water storage decreased by more than 80% and 28% in maples, but only by 31% and
31 1% in oaks. We suggest that the preferential use of deep water by red oaks allows the species to
32 continue transpiration and growth during soil water limitations. In this case, deeper roots may
33 provide a buffer against drought-induced mortality. Using 14 years of growth data, we show that
34 maple growth correlates with mean annual soil moisture at 30 cm, but oak growth does not. The
35 observed responses of oak and maple to drought were not able to be explained by leaf and xylem
36 physiology alone. We employed the FETCH2 plant-hydrodynamics model to demonstrate the
37 influence of root, stem, and leaf controls on tree-level transpiration. We conclude that all three
38 levels of hydraulic traits are required to define hydraulic strategy.

39

40 **Key words** *Acer rubrum*, Hydraulic strategy, Plant functional type, *Quercus rubra*, Sap flux,
41 Stable isotope analysis, Stem water storage, Plant hydrodynamic model

42

43

44

45

46

47

48

49

50

51 **Introduction**

52 Water availability limits transpiration and carbon uptake in plants (Dawson 1993, Horton
53 & Hart 1998). Plants regulate water status dynamically through controls at the leaf, stem, and
54 root levels. At the leaf level, stomata can close during water stress to maintain a steady, high leaf
55 water potential (isohydry); remain open while risking highly negative leaf water potentials to
56 maximize carbon uptake (anisohydry); or operate along a range of intermediate strategies
57 (McDowell et al. 2008, Skelton et al. 2015). At the stem level, conductive woody tissue differs in
58 the size and organization of conductive xylem vessels, leading to differences in maximum
59 conductivity (high vs. low) and the water pressure at which the onset of cavitation occurs
60 (cavitation resistant xylem vs. cavitation vulnerable xylem). Conductivity and vulnerability
61 typically correlate with the morphology of the xylem, with ring porous xylem tending to be more
62 conductive but more cavitation vulnerable, and diffuse porous xylem with lower maximum
63 conductivity but less cavitation vulnerable (Pockman & Sperry 2000). Conifers present a
64 tracheid-based morphology that may be more cavitation resistant than both angiosperm wood
65 types and have lower hydraulic conductivity than diffuse porous xylem (Sperry et al. 1994,
66 Choat et al. 2012). A third axis of hydraulic control results from the architecture of root systems
67 across different species. Species with deeper roots can access water at greater depths than are
68 unavailable to more shallowly rooted species (Jackson et al. 1996, Canadell et al. 1996).
69 Different species exhibit a spectrum of traits that vary in cavitation risk across all three of these
70 axes of hydraulic control (Figure 1) (Meinzer et al. 2014).

71 Regulation of water use is often considered to be primarily dominated by interactions
72 between xylem architecture and stomatal behaviour (McDowell et al. 2008). In many cases,
73 vascular structure and stomatal response strategies may co-vary to optimize water use and offset
74 risks associated with traits along the other axis (Manzoni 2014, Manzoni et al. 2014, Nolf et al.
75 2015). However, several counterexamples exist. For example, many species of trees operate
76 stomata anisohydrically, despite having more vulnerable ring-porous xylem (Martinez-Vilalta et
77 al. 2014, Thomsen et al. 2013). Yet, these trees rarely experience hydraulic limitations to
78 transpiration and some are quite drought resistant (Cochard et al. 1992). Therefore, the
79 combination of leaf and xylem traits may not be sufficient to explain plant water use dynamics.
80 This portends that root-level controls must also be considered to understand plant water use and
81 drought susceptibility. We term the syndrome of emergent phenotypic hydraulic functional traits

82 at the root, stem, and leaf levels as the whole-plant hydraulic strategy and posit its governing role
83 in not only plant- but also ecosystem-level water use (Matheny et al. 2016).

84 Differences among species in whole-plant hydraulic strategy promote distinct
85 transpiration rates and patterns (Dawson 1993, Dawson 1996, Meinzer et al. 1999, Nadezhdina et
86 al. 2008, McCulloh et al. 2012, Ford et al. 2011). It is common for species within the same
87 ecosystem to employ opposing hydraulic strategies (e.g., risk prone or risk adverse) (McCulloh
88 et al. 2012, Ford et al. 2011). Disparities in transpiration volume and timing, due to differences
89 in whole-plant hydraulic strategies employed within the same forest, have important implications
90 for forest growth and response to drought and disturbance (Roman et al. 2015, McDowell et al.
91 2008, Matheny et al. 2014b, Gao et al. 2015, Gu et al. 2015, Wullschleger et al. 1998). Several
92 water flux studies have shown that many species of ring-porous, anisohydric oak continue to
93 transpire after other species curtail their water use during mild to moderate drought (e.g. von
94 Allmen et al. 2014, Baldocchi & Xu 2007, Hernandez-Santana et al. 2008, Matheny et al.
95 2014b). To explain this observation, authors suggest that certain species of oaks may root more
96 deeply than co-occurring species, and therefore may access water pools that are unavailable to
97 other species. Although only a limited number of studies have looked directly into the
98 relationship between oak root water-uptake depth and transpiration, a few have shown the
99 importance of deep water access for drought resistance (Miller et al. 2010, Nadezhdina et al.
100 2008, Pinto et al. 2014, Phillips & Ehleringer 1995). Traits within the rhizosphere such as
101 rooting depth and vertical distribution, root length and diameter distribution, root-water uptake
102 efficiency, and mycorrhizal interaction have been shown to determine water acquisition and use
103 (Matheny et al. 2016, Canadell et al. 2007, Allen 2009). The hypothesized ‘safe’ rooting strategy
104 of oak may be the key that permits the high-risk combination of anisohydry and ring-porous
105 xylem in terms of the proposed plant hydraulic safety-efficiency trade off (Meinzer et al. 2010,
106 Manzoni et al. 2013, but see the counter argument presented by, Gleason et al. 2016). Deep
107 roots may also be the critical aspect of hydraulic strategy that provides additional drought
108 resilience to oak dominated ecosystems (Tognetti et al. 1998).

109 In a study of species-specific water relations, anisohydric, ring-porous red oak (*Quercus*
110 *rubra* L.) did not demonstrate the water-stress induced limitations to transpiration expected for
111 this combination of risk-prone hydraulic traits (Matheny et al. 2014b). For the same field site,
112 Thomsen et al. (2013) showed that red maple (*Acer rubrum* L.) exhibited an “ultra” safe strategy

113 combining isohydric stomatal regulation with diffuse porous xylem. Both studies postulate that
114 the observed sustained transpiration by red oaks during water stress may result from a deep
115 rooting strategy. Here, we examine the effects of potential rooting depth differences between red
116 oaks and red maples using stable isotope analysis of xylem water from both species. Stable
117 xylem water isotopes are useful tracers because they reflect the isotopic composition of source
118 water taken up by the roots (Walker & Richardson 1991, Ehleringer and Dawson 1992). Phase
119 changes associated with precipitation and evaporation unequally partition the heavy and light
120 isotopes of oxygen and hydrogen in water, promoting distinct isotope values across different
121 environmental water sources (Ehleringer & Dawson 1992, West et al. 2012, Gaines et al. 2015,
122 Gat 1996). We integrate our isotopic analysis with measurements of sap flow, stomatal
123 conductance, photosynthesis, and long-term growth to compare the performance of these two
124 species with respect to each of the three compartments of the whole-plant hydraulic strategy.

125 We use a tree-level hydrodynamic modeling framework to test the sensitivity of whole-
126 plant transpiration to different components of the hydraulic regulation system, inclusive of
127 different combinations of root, stem, and leaf traits on transpiration. This type of trait-based
128 approach to describing hydraulic strategy at the species-level could potentially inform the
129 representation of plant hydraulic function within plant-functional types in ecosystem and land-
130 surface models (Matheny et al. 2016). It has been shown that over-aggregation of functionally
131 distinct species, such as red oak and red maple, into the same plant functional type (e.g.
132 temperate broadleaf deciduous) leads to errors in short- and long-term predictions of water and
133 carbon fluxes (Poulter et al. 2011, Matheny et al. 2014a, Matthes et al. 2016). Recent efforts to
134 include plant hydraulic traits and the resultant hydrodynamics in ecosystem models have shown
135 promise for improving simulations of transpiration and alleviating some of these errors (Xu et al.
136 2016).

137 We hypothesize that (1) red oaks in northern Michigan are rooted more deeply than red
138 maples, and therefore can access a steady, deep supply of water that red maples cannot. (2) This
139 deep steady water supply permits red oaks to maintain transpiration when soil moisture within
140 the top 3 meters of the soil is depleted. (3) We expect that bole growth will be closely coupled
141 with surficial soil moisture (30 cm) in species whose overall transpiration is more limited by
142 hydraulic stress, such as red maples, but not red oaks. (4) We predict that each combinations of
143 leaf, stem, and root traits comprising different whole-plant hydraulic strategies, will lead to

144 different transpiration rates and will be sensitive to hydraulic limitations under different ranges
145 of environmental water stress.

146

147 **Materials and Methods**

148 *Site description*

149 This study was conducted within the footprint of the Ameriflux-affiliated eddy
150 covariance tower, US-UMB (45° 33' 35" N, 84° 42' 48" W, elev. 236 m) at the University of
151 Michigan Biological Station (UMBS) in northern lower Michigan, USA. The 30-year mean
152 annual precipitation for the region is 766 mm with a mean annual temperature of 5.5 °C
153 (Pellston, MI Regional Airport, NOAA National Climate Data Center). Local soils are well-
154 drained Haplorthods of the Rubicon, Blue Lake, or Cheboygan series, and are composed of
155 92.2% sand, 6.5% silt, and 0.6% clay (Nave et al. 2011). The UMBS forest is transitioning from
156 an early successional stage with bigtooth aspen (*Populus grandidentata* Michx.) and paper birch
157 (*Betula papyrifera* Marsh.) dominating the canopy, to a mid-successional forest with dominant
158 species of red maple (*Acer rubrum* L.), red oak (*Quercus rubra* L.), and white pine (*Pinus*
159 *strobus* L.). The average tree age is roughly 90 years, and mean canopy height is approximately
160 22 m. Mean peak leaf area index (*LAI*) is 3.9 m² m⁻² and mean stem density of mature trees
161 (diameter at breast height or DBH > 8 cm) is approximately 750 stems per hectare. Red maple
162 stems comprise 6.0 m² per hectare with an average DBH of 17.57 ± 5.9 cm. Red oak stems
163 account for 3.7 m² per hectare with an average DBH of 25.95 ± 10.3 cm. Trees selected for
164 physiological measurements in this study were representative of this species-size distribution of
165 the forest. While sap flux analysis measured a variety of sizes and canopy positions,
166 measurements of stem water storage, leaf properties, and xylem water isotopic composition were
167 all made on canopy dominant individuals in close proximity to each other. Additional site details
168 can be found in Gough et al. (2013).

169

170 *Meteorological data*

171 Meteorological measurements were collected at a 46 m eddy covariance tower (Gough &
172 Curtis 1999-). Air temperature, humidity, and atmospheric pressure were recorded every minute
173 and averaged to ten-minute block averages (HC-S3, Rotronic Instrument Corp. Hauppauge, NY,
174 USA and PTB101B, Vaisala, Helsinki, Finland). A quantum sensor (LI-190, LI-COR

175 Biosciences, Lincoln, NE, USA) measured incoming photosynthetically active photon flux
176 (PAR). A tipping bucket rain gauge (TE-525, Texas Electronics, Dallas, TX, USA) at the base of
177 the tower measured precipitation. Additional information regarding the instrumentation and
178 analysis approach of the meteorological data at the site are described in Gough et al. (2013) and
179 Maurel et al. (2013).

180

181 *Soil water potential*

182 Volumetric soil water content and temperature were recorded in four locations at depths
183 of 5, 15, 30, and 60 cm. Two of these locations also included measurements at 100, 200, and 300
184 cm depths (Hydra probe SDI-12, Stevens Water Monitoring Systems, Inc., Portland, OR, USA)
185 (He et al. 2013). Soil moisture is reported as an average across all sensors at the same depth.
186 Following the procedures outlined by He et al. (2013), soil moisture measurements were
187 corrected for systematic bias, estimated for our site to as $\sim 0.03 \text{ m}^3 \text{ m}^{-3}$, and smoothed using a 10
188 hour moving average. Soil water content (θ , $\text{m}^3 \text{ m}^{-3}$) was vertically integrated over the 3 m soil
189 column. Soil water potential (Ψ_s , MPa) was calculated at each depth from soil moisture data
190 using the van Genuchten (1980) hydraulic parameterization. Soil hydraulic parameters were
191 derived from pedo transfer functions using the percentages of sand, silt, and clay (92%, 7%, and
192 1%) for our plots (He et al. 2013).

193

194 *Sap flux*

195 Sap flux was monitored in red maple ($n = 8$) and red oak ($n = 10$) via Granier-style
196 thermal dissipation probes (Granier 1987) (Table 1). Sap flux trees were selected to capture a
197 variety of sizes and canopy positions to enable analysis at the plot-scale for comparison with
198 eddy covariance measurements. Pairs of 20 mm long probes were inserted into the sapwood at
199 breast height, and the upper probe was continuously supplied with 0.2 W of heating power. Data
200 were recorded every minute and averaged to half-hour intervals. For trees where the sapwood
201 depth was less than the 20 mm sensor length, we applied the Clearwater et al. (1999) correction.
202 Sensor data were processed using a baselining procedure, using periods when the two-hour
203 average vapor pressure deficit (VPD) was less than 0.5 kPa to allow for nightly recharge flow
204 (Oishi et al. 2008). Baselines were determined with respect to the maximum nocturnal

205 temperature for each sensor in order to account for any variation between sensors. Voltage
206 differences between each pair of probes were converted to sap flux density (J_s , $\text{g H}_2\text{O m}^{-2}_{\text{sapwood s}^{-1}}$
207 $^{-1}$) following Granier (1985). Sapwood depth at breast height was estimated from species- and
208 plot-specific allometric equations developed by Bovard et al. (2005) and Matheny et al. (2014b).
209 Sap flux density was converted to sap flow (g s^{-1}) by multiplying J_s by the sapwood area of the
210 individual tree. Data collected in this experiment were part of a larger study of plot-level sap flux
211 ($n = 42$ trees of 5 species). During the 2014 growing season, plot-scaled sap flux comprised 78%
212 of latent heat flux as measured through eddy covariance. Full details of the plot-level sap flux
213 experiment are described in Matheny et al. (2014b).

214 *Stem water storage*

215 Stem water storage was continuously monitored in one mature, canopy-dominant
216 individual of each species, red oak and red maple, from 10 July until 14 September 2014 (day of
217 year, DOY 191-257). Ruggedized soil moisture sensors (model GS-3, Decagon Devices,
218 Pullman, WA, USA) were installed at two different heights: at the base of the trunk (0.5 m above
219 the ground) and just below the live crown (~5.5 m from the ground). Conductive tissue depth
220 was estimated at each sensor location using the measured diameter at that location in place of
221 DBH with the sapwood-DBH allometry provided for the site (Bovard et al. 2005, Matheny et al.
222 2014b). To avoid heartwood penetration past the red oak's shallow sapwood depth, sensor tines
223 were trimmed to the depth of sapwood for each location. Dielectric potential was recorded by the
224 stem water storage sensors via frequency domain reflectometry every minute and averaged to the
225 half hour. Prior to installation, stem water storage sensors were calibrated to the different
226 densities of oak and maple wood (Matheny et al. 2015). These species-specific calibration
227 equations were then used to convert dielectric potential to volumetric water content (VWC). Stem
228 storage (kg) was calculated for each tree by integrating VWC over the conductive volume of the
229 bole. Full details of sensor calibration, installation, and data processing are provided in Matheny
230 et al. (2015).

231 232 *Leaf-level measurements*

233 Leaf water potential was measured in canopy-top leaves of mature red oak and red maple
234 trees exposed to full sun using a pressure chamber (Model 600 PMS Instrument Co., Corvallis,

235 OR, USA). Leaves were accessed via a mobile canopy lift. Two leaves from each species were
236 tested three times per day from 23 June to 12 July 2014 (DOY 174-193). Measurements were
237 made at roughly 6:00 ('dawn'), 13:30 ('noon'), and 16:00 ('afternoon'). Directly prior to
238 measurement, the petiole was cut and inserted into the compression gasket, which was then
239 tightened securely around the stem. Internal chamber pressure was increased until moisture was
240 visible on the petiole. The corresponding pressure was denoted as Ψ_L (MPa).

241 Leaf-level stomatal conductance and photosynthesis were observed *in situ* on the same
242 trees from which leaf water potential was measured. Conductance and photosynthesis were
243 measured using a portable infrared gas analyzer (IRGA) (LI-6400, LI-COR Biosciences,
244 Lincoln, NE, USA). One leaf per species was measured daily at 13:30 ('noon') and 16:00
245 ('afternoon'). Each leaf was measured four times per sampling period with a replication rate of
246 30 s. Ambient CO₂ inside the chamber was set at 370 ppm, controlled by the LI-6400 CO₂
247 injection system, and humidity was adjusted with chemical scrubbers to 50%. Leaf temperature
248 was set to 28 °C using the LI-6400 built-in temperature regulator, while ambient radiation was
249 used and recorded. Average leaf temperature during measurement was 27.4 ± 2.5 °C for red
250 maples and 27.1 ± 2.9 °C for red oaks. Mean relative humidity during measurement was $47.2 \pm$
251 7.3% and $49.8 \pm 7.9\%$ for red maples and oaks respectively. Intrinsic water use efficiency
252 (WUE) was calculated from the cuvette data as carbon gain normalized by stomatal conductance.

253

254 *Tree growth measurements*

255 Bole growth information is collected annually via dendrometer bands located at breast
256 height on a random subset of trees of all species (n = 933) including red maple (n = 423) and red
257 oak (n = 114) (Gough et al. 2010). Measured end-of-season diameters are converted to bole
258 areas, A (cm²), for each year (i) for all years from 2001 to 2014. Annual percent bole growth per
259 tree is calculated using Equation (1). Only trees with a DBH greater than 8 cm at the beginning
260 of the 14 year period were included in this analysis. Mean annual bole growth is calculated as
261 the mean of the annual percent bole growth over all trees of each species.

$$262 \text{ Growth} = \left(\frac{A_{i+1} - A_i}{A_i} \right) * 100\% \quad (1)$$

263

264 *Xylem water isotopes*

265 Tree cores were extracted using an increment borer from multiple mature, canopy-
266 dominant maple and oak individuals in June, July, and August 2014. To avoid damage from
267 repetitive coring to trees instrumented with sap flow or storage sensors, trees of similar species
268 and size within the same plot were selected. We designed our sampling to constrain within- and
269 between-species variability in addition to temporal variability. On 29 June 2014 (DOY 180), we
270 collected cores from five oaks and four maples to sample within-species variability. To monitor
271 temporal variability, we collected cores from two individuals of each species daily from 9-13
272 July (DOY 190-194) and 4-8 August (DOY 216-220). Extracted cores were placed in 20 mL
273 scintillation vials with a poly-cone lined cap (Wheaton, Millville, NJ, USA) and kept frozen at -
274 80 °C until analysis.

275 The isotopic composition of xylem water in the cores was determined using a Picarro
276 L2120-T Cavity Ringdown Spectrometer (CRDS) coupled to a Picarro A0213 Induction Module
277 (IM, together, IM-CRDS). Samples were prepared for the IM by placing a ~1 mm thick slice of
278 xylem into a folded metal strip and loading the xylem-strip assembly into a glass vial purged
279 with zero dry air. Water is extracted by the IM via heating with a programmed induction coil. A
280 carrier stream of zero dry air transports the evaporated water to the analyzer. The CRDS software
281 package (Picarro, Inc., Santa Clara, CA, USA) calculates the isotopic composition of the sample
282 as a mass-weighted integral across the peak. We calibrated measured isotopic compositions to
283 the Vienna Standard Mean Ocean Water (VSMOW) standard (e.g., Coplen 1996) using lab
284 standards of known isotopic composition. To perform the calibrations, we transferred 4 μ L of
285 our internal lab standards onto a piece of glass filter paper, and loaded the filter paper into a
286 metal sample holder identical to those used to analyze the cores. We then measured the isotopic
287 composition of water in the filter paper using an identical procedure as used for the tree cores.
288 From these values, we developed a linear transfer function from measured analyzer values to the
289 VSMOW scale. All tree core samples and standards were analyzed a minimum of three times.
290 We express our isotopic compositions in delta notation as part-per-thousand deviations from the
291 VSMOW standard (e.g., $\delta = 1000[(R_{sample}/R_{VSMOW}) - 1]$, where R is the heavy-to-light
292 stable isotope ratio). Median standard errors across all xylem samples were 0.3‰ for $\delta^{18}\text{O}$ and
293 1.1‰ for δD . Deuterium excess ($d = \delta\text{D} - 8\delta^{18}\text{O}$), which is typically thought to reflect the
294 magnitude of kinetic fractionation, is calculated following the definition by Dansgaard (1964).
295 Lower values of d in xylem water indicate a more evaporated, surficial soil water source while

296 higher values of d indicate water less affected by evaporation, such as deep soil water or
297 groundwater (Simonin et al. 2014).

298 The IM-CRDS method is faster and less expensive on a per-sample basis than traditional
299 cryogenic distillation techniques (e.g., Ehleringer *et al.*, 2000). However, the technique is new
300 and therefore, the data require careful consideration (e.g., Berkelhammer *et al.*, 2013). We
301 outline below four potential concerns. First, volatile organic compounds in the tree core samples
302 can interfere with spectroscopic isotopic measurements, including CRDS techniques (West *et al.*,
303 2011). This bias results from spectroscopic overlap of wavelengths absorbed by both water and
304 organic molecules. The IM seeks to minimize this potential bias by removing organic molecules
305 through: (a) adsorption to a heated activated carbon column and (b) oxidation by a
306 micropyrolysis column maintained at 1200°C (e.g., Berkelhammer *et al.*, 2013). Second, isotopic
307 values in CRDS measurements depend weakly on water vapor concentration, and the correction
308 varies by instrument and can vary through time (Tremoy *et al.*, 2011). To minimize the potential
309 influence of this bias, we optimized the IM heating recipe to our samples such that: (a) water
310 vapor concentrations were kept as constant as possible through the peak and (b) peak shapes
311 were similar across maple, oak, and standard samples. Third, isotopic memory effects can
312 influence measured compositions (e.g., Berkelhammer *et al.*, 2013, Gupta *et al.*, 2009).
313 Instrumental memory occurs when residual vapor from prior analyses remains in the analyzer
314 cavity, and is measured during subsequent analyses. The influence of memory on the measured
315 isotopic value depends on the magnitude of isotopic difference between subsequent samples. We
316 monitored for instrumental memory effects by looking for a linear trend in the isotope values
317 from the first few analyses of a sample, and we discarded the values where strong memory
318 effects were apparent. We observed the strongest memory effects between samples of the lab
319 standards used, which were more isotopically distinct from each other than the maple and oak
320 samples were from each other. Therefore, we expect the implications of instrumental memory to
321 be small. Finally, water extraction by IM-CRDS is sensitive to the rate and duration of sample
322 heating. Ideally, the induction coil should heat the sample just until all of the water is removed.
323 The sample may combust with further heating, leading to water isotope values that are biased by
324 combustion-derived water. We monitored our analyses for combustion through visual inspection
325 of the core sample for charring and of the analyzer peaks following analysis. Combustion water
326 introduces a long tail to the water concentration peak and marked deviations in measured isotope

327 values. Analyses that were influenced by combustion were omitted. While we strived to
328 minimize instrumental bias from known sources, we note that the IM-CRDS procedure has yet to
329 undergo extensive validation. Regardless, we maintain that our xylem water measurements
330 record environmental water sources and variability as xylem water compositions closely match
331 local environmental waters, and measurements across all samples were consistent.

332

333 *Analysis of liquid water samples*

334 We collected samples of local precipitation and nearby surface and ground waters to
335 constrain the isotopic composition of likely tree water sources. Surface and ground water
336 samples were collected in 20 mL scintillation vials and were sealed with a poly-cone lined cap
337 until isotopic analysis. We collected surface water from Douglas Lake on UMBS property and a
338 stream ~1 km southwest of Douglas Lake. Four precipitation samples were collected
339 approximately biweekly from mid-June until mid-August in a bucket with a layer of mineral oil
340 to prevent evaporation (Scholl et al. 1996, Friedman et al. 2002). We collected precipitation
341 from the bucket by using a syringe to extract precipitation from below the layer of mineral oil.
342 After collection, the bucket was emptied, cleaned, dried, and a layer of mineral oil replaced for
343 the next sample.

344 We analyzed the isotopic composition of the liquid samples with a Picarro L2120-i
345 CRDS coupled to an A0211 high precision vaporizer and attached autosampler. We monitored
346 for organic contamination using the Picarro ChemCorrect software (e.g., West et al. 2011).
347 Standard errors for liquid water $\delta^{18}\text{O}$ and δD were below 0.1 ‰ and 0.4 ‰, respectively.

348

349 *Sensitivity analysis*

350 We conducted a sensitivity analysis using the Finite-difference Ecosystem-scale Tree
351 Crown Hydrodynamics model version 2 (FETCH2) (Mirfenderesgi et al. 2016). FETCH2
352 approximates water flow through a tree's xylem system as flow through unsaturated porous
353 media (Sjerry et al. 1998) with conductance and capacitance changing dynamically in response
354 to stem water potentials. A full model description and formulation are provided in Mirfenderesgi
355 et al. (2016) and Bohrer et al. (2005). We tested all eight combinations of each studied opposing
356 trait pair along the three axes of hydraulic control (Figure 1): (1) deep roots, anisohydric stomatal
357 regulation, ring porous wood; (2) deep roots, anisohydric stomatal regulation, diffuse porous

358 wood; (3) deep roots, isohydric stomatal regulation, ring porous wood; (4) deep roots, isohydric
 359 stomatal regulation, diffuse porous wood; (5) shallow roots, anisohydric stomatal regulation, ring
 360 porous wood; (6) shallow roots, anisohydric stomatal regulation, diffuse porous wood; (7)
 361 shallow roots, isohydric stomatal regulation, ring porous wood; (8) shallow roots, isohydric
 362 stomatal regulation, diffuse porous wood.

363 FETCH2 incorporates plant traits at the leaf, stem, and root levels through suites of
 364 parameters affecting water transport at each level. Two leaf trait parameters, C_3 and Φ_σ , define
 365 stomatal response to leaf water potential and can be tuned to represent isohydry and anisohydry.
 366 Φ_σ is the inflection point in the stomatal response to xylem water potential (MPa), C_3 is a unitless
 367 shape parameter for stomatal response to xylem water potential, and n represents the model's
 368 time step. We approximated values for these parameters based on leaf water potential data for
 369 red oaks and red maples in our site reported in the present study and by Thomsen et al. (2013)
 370 (Table 2 and Figure 2).

$$371 \quad \beta = \frac{E^{(n)}}{E^{(n)}_{v,max}} = \exp \left[- \left(\frac{\Phi^{(n-1)}}{\Phi_\sigma} \right)^{C_3} \right] \quad (2)$$

372 Where β is the response of stomatal conductance to changes in xylem water potential, $E^{(n)}_v$ is the
 373 FETCH2 calculated actual transpiration (g s^{-1}), $E^{(n)}_{v,max}$ is the half-hourly potential evaporative
 374 demand determined from canopy top atmospheric conditions used to force the model (g s^{-1}), Φ is
 375 the xylem water potential calculated by the FETCH2 model (MPa).

376 Parameters that describe stem level traits, Φ_{50} and Φ_{88} , represent the xylem water
 377 potentials (MPa) at 50% and 88% relative water content (RWC) respectively, and are used to
 378 describe the capacitance in response to changing xylem water potentials. Due to the paucity of
 379 measurements of RWC alongside stem water potential in the literature, values for Φ_{50} and Φ_{88}
 380 were approximated on the basis of observed reliance on stem water storage in this study and the
 381 values obtained through model optimization by Mirfenderesgi et al. (2016) for oak species
 382 (Table 2 and Figure 2).

$$383 \quad RWC = 1 + \frac{\Phi}{(b\Phi - \Phi_{50}(2+b))} \quad (3)$$

384 Where b is calculated as follows:

$$385 \quad b = \frac{\Phi_{88} - 0.24\Phi_{50}}{0.12(\Phi_{50} - \Phi_{88})} \quad (4)$$

386
387 K_{max} ($\text{kg m}^{-1} \text{s}^{-1} \text{MPa}$), C_1 (MPa), and C_2 , represent the maximum xylem conductance and the
388 shape of the xylem vulnerability curve, respectively, and are used to calculate dynamic changes
389 in actual xylem conductance, K ($\text{kg m}^{-1} \text{s}^{-1} \text{MPa}$). Together, these stem level traits represent the
390 effects of xylem architecture on transpiration. Values used for K_{max} were reported by Maherali et
391 al. (2006) for red oak and red maple in Duke Forest in Durham, NC (Table 2).

$$392 \quad K = A_{\text{sapwood}} K_{\text{max}} \exp \left[- \left(\frac{-\Phi}{C_1} \right)^{C_2} \right] \quad (5)$$

393 Where A_{sapwood} refers to the sapwood area of the tree (m^2). C_1 and C_2 , were calculated from
394 reconstructed xylem vulnerability curves for red oak and red maple using the observed values for
395 50 and 88 percent conductivity loss provided in the database xylem water potentials compiled in
396 Choat et al. (2012, Supplemental material) (Table 2 and Figure 2). For this analysis, all
397 structural properties of the simulated tree (e.g. sapwood area, crown area, leaf area index,
398 vertical distribution of leaves, tree height, diameter at breast height, stem taper) were held
399 constant to allow for isolated, direct comparisons of the effects of differing hydraulic parameter
400 sets.

401 Because FETCH2 lacks an explicit representation of the root component we prescribed
402 water potentials to serve as the model's boundary condition for the top of the root system and
403 base of the stem. We represented deep roots by prescribing a constant high water potential, -
404 0.033 MPa, typically referred to as field capacity (Rawls et al. 1982). A shallow rooting strategy
405 was simulated by water potential that steadily declined over the seven day dry-down simulation
406 period from -0.033 MPa (field capacity) to -1.5 MPa (the permanent wilt point (Rawls et al.
407 1982)) (Figure 2). We forced the model using potential transpiration calculated from the above
408 canopy conditions as measured at our field site on 17 July 2013, a sunny day with minimal cloud
409 cover and low to moderate VPD (maximum half-hourly PAR = $1,817.5 \mu\text{mol m}^{-2} \text{s}^{-1}$, mean
410 temperature = $27.6 \text{ }^\circ\text{C}$, maximum half-hourly VPD = 2.6 kPa). We recycled these conditions for
411 seven simulation days. Potential transpiration was determined following Mirfenderesgi et al.
412 (2016, Appendix A).

413

414 Results

415 During the peak growing season of 2014, between 10 July (DOY 191) and 30 September
416 (DOY 273), daily peak sap flux averaged $40.8 \pm 14.3 \text{ g m}^{-2} \text{ s}^{-1}$ for red maples and $39.8 \pm 12.4 \text{ g}$
417 $\text{m}^{-2} \text{ s}^{-1}$ for red oaks. During this period, stem-stored water use averaged $4.8 \pm 2.9 \text{ kg day}^{-1}$ in red
418 maple, and $2.9 \pm 2.4 \text{ kg day}^{-1}$ in red oak. Withdrawal from storage, or the diurnal fluctuation in
419 the amount of stem-stored water, was largest in red maples when soil water was non-limiting,
420 and tended to be between 5 and 10 kg day^{-1} . Intrinsic WUE for red maple ($101.1 \mu\text{mol CO}_2 \text{ mol}^{-1}$
421 H_2O) exceeded that of red oak ($84.1 \mu\text{mol CO}_2 \text{ mol}^{-1} \text{H}_2\text{O}$) by 16.9%.

422 Soil water content decreased by 20% from DOY 211-223 (30 July – 11 August),
423 constituting a 2-week "mini-drought" (Figure 3A). Red maple sap flux and stem water storage
424 were strongly affected by this decrease in soil water content, while red oak water fluxes were
425 not. During this period of limited soil moisture, mean daily maximal sap flux in red maples fell
426 from $59.8 \pm 30.6 \text{ g m}^{-2} \text{ s}^{-1}$ (at DOY 211) to $11.5 \pm 6.4 \text{ g m}^{-2} \text{ s}^{-1}$ (at DOY 223), a reduction of over
427 80%. For the same time period, maximum daily sap flux from red oaks declined by only 31%,
428 from $45.7 \pm 14.9 \text{ g m}^{-2} \text{ s}^{-1}$ to $32.4 \pm 10.6 \text{ g m}^{-2} \text{ s}^{-1}$ (Figure 3B). Concurrently, maximum daily
429 stem water storage in red maple fell by 28% from 100.0 kg to 72.1 kg, while remaining nearly
430 constant (between 108.3 kg and 107.2 kg, i.e., <1% decrease) in red oak (Figure 3C). During the
431 "mini-drought," diurnal withdrawal from storage by red maple fell from 13.4 kg on DOY 213 to
432 0.78 kg on DOY 222. Red oaks demonstrated an opposing pattern. Daily storage withdrawal in
433 red oaks ranged from 0 to 5 kg when soil water was non-limiting, but rose from 4.0 kg on DOY
434 211 to 8.4 kg on DOY 222.

435 To isolate the effect of soil water content on sap flux, we first conducted a multiple linear
436 regression between integrated daily sap flux, total daily PAR, and daily maximum VPD ($R^2 =$
437 0.268 and 0.274 for red maple and red oak respectively, $P < 0.0001$ for both). We used the
438 residual sap flux from this regression model to calculate a second linear regression against Ψ_s at
439 every measurement depth between 5 and 300 cm ($n = 7$) (Table 3). Due to the non-linear nature
440 of Ψ_s , we used an inverse log function of the absolute value of Ψ_s to linearize the data following
441 Thomsen et al. (2013). Residual sap flux from red maples demonstrated significant relationships
442 with Ψ_s at every depth except 5 and 200 cm, with the most strongly correlated relationship
443 occurring at 30 cm ($P < 0.0001$, $R^2 = 0.20$) (Table 3). Residual sap flux from red oaks was
444 weakly (though significantly) related to Ψ_s , and only at 300 cm ($P = 0.0272$, $R^2 = 0.05$) (Table 3).
445 Soil moisture between 5 and 100cm is strongly auto-correlated (mean $R^2 = 0.75$, $P < 0.0001$).

446 Soil moisture at 200 cm is well correlated with that at 300 cm ($R^2 = 0.57$, $P < 0.0001$) but is less
447 well correlated with that in the overlying layers (mean $R^2 = 0.26$, $P < 0.0001$). It is possible that
448 red maples draw upon water throughout the shallow soil column, but the autocorrelation between
449 soil moisture in the shallow layers prevents us from pinpointing precisely where maple root-
450 water uptake occurs. However, these results do suggest that oak water uptake occurs at a deeper
451 location than maple water uptake.

452 Leaf water potential measurements illustrated that each species used different leaf
453 hydraulic strategies. Red maples possessed a narrow range of Ψ_L between -0.12 and -1.2 MPa
454 over the 20-day measurement period. Red oaks showed a larger range, -0.13 to -2.2 MPa, almost
455 double of that of maples during the same period. Red maple Ψ_L was not strongly affected by
456 VPD (Figure 4); the only significant relationship between Ψ_L and VPD ($P = 0.0335$, $R^2 = 0.21$)
457 occurred in the late afternoon (16:00, Figure 4C). Conversely, red oaks demonstrated strong
458 correlations between VPD and Ψ_L during noon-time (13:00, Figure 4D) ($P = 0.0040$, $R^2 = 0.46$)
459 and late afternoon (16:00) ($P = 0.0117$, $R^2 = 0.3195$, Figure 4F). Predawn Ψ_L was not correlated
460 with VPD for either species ($P > 0.1$).

461 Oak xylem water exhibited more consistent isotopic compositions than maple xylem
462 water (Figure 5A, B). Maple xylem delta values varied substantially from month to month, while
463 oak xylem isotope compositions did not. For June, July, and August, mean maple compositions
464 were -8.8 ± 0.2 , -7.2 ± 0.2 , and -9.6 ± 0.1 ‰ for $\delta^{18}\text{O}$ respectively, and -76.3 ± 0.8 , -65.0 ± 0.4 ,
465 and -78.9 ± 0.3 ‰ for δD . In contrast, mean oak xylem compositions for the same time period
466 were -10.6 ± 0.2 , -10.7 ± 0.2 and -10.5 ± 0.1 ‰ for $\delta^{18}\text{O}$ and -81.7 ± 0.6 , -81.4 ± 1.0 , and $-78.4 \pm$
467 0.4 ‰ for δD . We did not observe any isotopic trends on a day-to-day basis during July and
468 August when cores were collected over multiple days.

469 Environmental water source compositions bracket the observed xylem water
470 compositions. Precipitation compositions were the most variable, ranging from -5.98 to -10.76
471 ‰ in $\delta^{18}\text{O}$ and -30.62 to -71.19 ‰ in δD from June to August. In contrast, surface water samples
472 collected from Douglas Lake and from the nearby stream were isotopically invariant. Douglas
473 Lake water samples ranged from -9.35 to -9.15 ‰ in $\delta^{18}\text{O}$ and -67.49 to -65.68 ‰ in δD , while
474 samples from the stream ranged from -9.38 to -9.50 ‰ in $\delta^{18}\text{O}$ and -67.28 to -69.19 ‰ in δD .
475 Finally, we measured the isotopic composition of deeper ground waters from three wells located
476 at the UMBS site. The shallower wells (25 and 47 m depth) had isotopic compositions of -8.12

477 and -8.28 ‰ for $\delta^{18}\text{O}$ and -59.88 and -60.59 ‰ for δD , while the deeper well (130 m depth) had
478 an isotopic composition of -13.18 ‰ for $\delta^{18}\text{O}$ and -87.5 ‰ for δD . All xylem water samples had
479 lower deuterium excess values than any of the observed precipitation values, with red maple
480 xylem water having substantially lower deuterium excess than that of red oaks (Figure 6).

481 We analyzed incremental bole growth records from 2001-2014 for both species with
482 respect to mean annual soil moisture at 30 cm and total annual precipitation. Because
483 instrumentation at additional soil depths (60 cm and beyond) was not installed until 2010, we
484 were limited in this analysis to soil moisture at 30 cm depth. For both species, mean annual bole
485 growth was uncorrelated with total annual and total growing season rainfall (all $P > 0.1$). Mean
486 annual soil moisture at 30 cm was not correlated with total annual rainfall ($P > 0.1$). Bole growth
487 was not correlated with mean growing season soil moisture. Bole growth of red maples was
488 positively correlated with mean annual soil moisture ($P = 0.0243$, $R^2 = 0.36$), while red oak
489 growth was uncorrelated with mean annual soil moisture ($P = 0.08$) (Figure 7). Among a sub-
490 sample of trees with the highest growth rates ($8 \text{ cm} < \text{DBH} < 20 \text{ cm}$) this relationship was still
491 stronger in maples ($P = 0.0176$, $R^2 = 0.40$ for red maples and $P = 0.31$ for red oaks). For the five
492 years of deep soil moisture measurement data (2010-2014), red maple bole growth was
493 correlated with mean annual soil between 15 and 300 cm with an average R^2 of 0.26. During this
494 period, bole growth for red oak was uncorrelated with mean annual soil moisture at all depths
495 (All $R^2 < 0.09$).

496 A sensitivity analysis was performed using FETCH2 to test the influence of suites of plant traits
497 at the leaf, stem, and root levels on diurnal transpiration patterns. We used observed plant trait values for
498 red oaks and red maple when they were available (Maherali et al. 2006, Choat et al. 2012, Thomsen et al.
499 2013), though we aim to compare the influence of traits at each level and the potential interactions
500 between them rather than to replicate the exact behavior of our studied trees. In the test case for ‘deep
501 roots,’ the combinations of anisohydry and ring porous xylem (simulation case #1, roughly representative
502 of the trait combination in red oak) allowed the highest transpiration rates relative to other trait
503 combinations. Anisohydry paired with diffuse porous xylem (simulation case #2) and isohydry paired
504 with ring porous xylem (simulation case #3) yield similar predicted transpiration, while the
505 isohydry/diffuse porous xylem combination (simulation case #4) exhibits the lowest predicted
506 transpiration (Figure 8).

507 For simulations using drying soil conditions, considered representative of a ‘shallow rooting’
508 strategy during an inter-storm dry-down period (simulation cases #5-8) (Figure 8), the trait combinations

509 representing anisohydry paired with ring porous wood (simulation case #5) produced the largest
510 simulated transpiration. Transpiration from isohydric/ring porous (simulation case #7) and
511 anisohydric/diffuse porous (simulation case #6) combinations began at relatively similar levels when soil
512 water was abundant (Figure 8), but the two trait pairs diverge as soil moisture declines, with the
513 isohydric/ring porous combination curtailing transpiration more quickly than the anisohydric/diffuse
514 porous combination (Figure 8). Transpiration predicted for the isohydric diffuse porous (simulation case
515 #8, roughly representative of the trait combination in red maple) species remained the lowest of the four
516 tested combinations. The isohydric/ring porous simulation (simulation cases #3 and #7) displayed
517 relatively flat transpiration throughout the course of the day regardless of soil (root) water access, typical
518 of the isohydric stomatal strategy. The three remaining leaf and xylem trait combinations (anisohydry/ring
519 porous, isohydry/diffuse porous, and anisohydry/diffuse porous) for both deep and shallow root cases
520 (Figure 5) all demonstrate a diurnal water flux skewed toward the morning hours, with the
521 anisohydry/diffuse porous case (simulation cases #2 and #6) as the most extreme.

522

523 Discussion

524 *Stem strategy*

525 While red oaks and red maples perform comparably under well-watered conditions,
526 differences in hydraulic strategies and controls lead to disparate trends in water flux when soil
527 moisture is low. During periods of adequate soil moisture, sap flux was greater in red maples
528 than in red oaks (Figure 3). Similar trends were shown for these species in our site in a previous
529 study conducted by Bovard et al. (2005), as well as for different species of oak and maple at
530 other sites (Oren & Pataki 2001, von Allmen et al. 2014). However, when soil moisture was
531 limiting, sap flux and stem water storage declined substantially in red maples but not in red oaks.
532 In a concurrent study, stem water storage and daily storage withdrawal in red maples were
533 significantly correlated with Ψ_s (Matheny et al. 2015). Likewise, after controlling for the effects
534 of PAR and VPD, residual sap flux in red maples was significantly correlated with Ψ_s at multiple
535 shallow depths, while residual sap flux in red oaks was correlated with Ψ_s at only 300 cm (Table
536 3). In oaks, sap flux and stem water storage were only moderately impacted by the mini-drought,
537 while both declined by large degrees in maples (Figure 3). Matheny et al. (2015) found that stem
538 water storage in oaks was only significantly positively correlated with Ψ_s when soil was wettest,
539 and that a negative correlation existed between withdrawal from storage and Ψ_s , indicating that
540 oaks relied upon stem-stored water for transpiration during times of depleted soil water only.

541 Conversely, red maples were found to rely heavily on daily withdrawal from storage to supply
542 the diurnal transpiration stream (Matheny et al. 2015). The limited reliance on diurnal storage
543 withdrawal by red oak, and the larger reliance on stored water by red maple, are consistent with
544 observations made in other ring- and diffuse-porous species (Wullschleger et al. 1996, Kocher et
545 al. 2015). Meinzer et al. (2013) similarly revealed that in a mixed deciduous forest in
546 Pennsylvania, diffuse-porous species were twice as sensitive to changes in soil moisture as co-
547 occurring ring-porous trees.

548

549 *Leaf strategy*

550 In addition to their xylem architecture differences, red oaks and red maples exhibit
551 distinct patterns of stomatal regulation. Although iso- and anisohydry are typically discussed
552 with respect to Ψ_s , we aim to create a discussion of whole-plant hydraulics where water status in
553 each organ is linked, in order, along the soil-root-stem-leaf-atmosphere continuum. Therefore,
554 we chose to relate Ψ_L to the atmospheric VPD during each measurement period (following
555 stomatal optimization theory), rather than directly to soil moisture (following cohesion-tension
556 theory) (Novick et al. 2015). The strong noon and afternoon correlations between Ψ_L and VPD in
557 red oak are characteristic of an anisohydric hydraulic strategy, where transpiration is sustained at
558 highly negative Ψ_L (Figure 4D, F). In contrast, the weak relationship between Ψ_L and VPD
559 during the afternoon in red maple represents a more isohydric strategy (Figure 4E). These results
560 agree with the traditional method of comparing Ψ_L to Ψ_s (Thomsen et al. 2013). In a synthesis
561 analysis, 12 out of the 13 *Quercus* species studied exhibited anisohydric stomatal regulation,
562 despite the increased embolism vulnerability associated with ring-porous xylem (Martinez-
563 Vilalta et al. 2014). Maherali et al. (2006) demonstrated that species with more vulnerable xylem
564 architectures, including seven species of *Quercus*, tended to have higher stomatal conductance
565 and photosynthetic rates. Under all soil water conditions, leaf WUE was greater in red maples
566 than in red oaks. Similarly, higher WUE has been documented in isohydric genotypes of poplars
567 than their anisohydric counterparts (Attia et al. 2015). Higher WUE is expected for isohydric
568 species that limit stomata opening to times when VPD is low, causing less water loss from the
569 stomata per unit CO₂ assimilated.

570

571 *Root strategy*

572 Several studies postulate that a deep rooting strategy allows oaks to maintain
573 transpiration at low Ψ_L in spite of their risk-prone vasculature and anisohydric stomatal
574 regulation strategies (e.g. von Allmen et al. 2014, Bovard et al. 2005, Oren & Pataki 2001,
575 Matheny et al. 2014b, Thomsen et al. 2013, Abrams 1990, Baldocchi & Xu 2007, Hernandez-
576 Santana et al. 2008). However, few offer clear evidence of water uptake from deep roots (Miller
577 et al. 2010, Phillips & Ehleringer 1995). Our xylem water isotope measurements indicate
578 differential water uptake between the two species with oaks preferentially take up more water
579 from deeper roots than maples. The more consistent isotopic compositions observed in red oak
580 xylem water relative to that in red maple imply that oaks obtain water from a more consistent
581 water source than maples (Figure 5). The isotopic variability of soil water decreases with depth
582 in the soil column (e.g. Barnes & Turner 1998, Breecker et al. 2009). Near the surface, the
583 isotopic composition of soil water reflects a balance between precipitation and evaporation, and
584 can change substantially after individual precipitation events (e.g. Gazis & Feng 2004, Barnes &
585 Allison 1988). For our site, the standard deviation around the mean seasonal soil moisture
586 declines dramatically below 100 cm (Table 3). We interpret this depth to be near the threshold of
587 extent for large evaporation effects on soil moisture. During dry interstorm periods, evaporation
588 from the soil surface enriches the residual water in heavy isotopes. As a result, soil water above
589 ~100 cm shows strong isotopic change on timescales of days to weeks. In contrast, isotopic
590 compositions of deeper soil water (> ~100cm) exhibit less variability since they are not subject
591 to the direct effects of evaporation, and water infiltrates to these depths only during large
592 precipitation events (Barnes & Turner 1998). Xylem water isotopes of red maple were observed
593 to vary strongly throughout the season, and track towards precipitation compositions (Figure 5,
594 Figure 6). This suggests that red maples predominantly use shallow water sources, consistent
595 with the high correlations observed between sap flux and Ψ_s from ~15-100 cm (Table 3). In
596 contrast, red oak xylem water compositions are more constant throughout the growing season,
597 implying a deeper, less variable water source (Figure 5, Figure 6). This is consistent with the
598 observation that sap flux is only significantly correlated with the deepest Ψ_s measured (300 cm,
599 Table 3).

600 The relationship between the $\delta^{18}\text{O}$ and δD compositions in extracted xylem water
601 provides additional isotopic evidence for water source differentiation. Evaporation from the top
602 soil layers fractionates H_2^{18}O relative to H_2^{16}O more than HD^{16}O relative to H_2^{16}O as a result of

603 the larger mass difference between the former pair of isotopologues compared to the latter.
604 Therefore, evaporated water will deviate strongly from the meteoric water line, and have lower
605 deuterium-excess values (d-excess, $d = \delta D - 8\delta^{18}O$). Several studies have shown that rooting depth
606 can be inferred from the d-excess parameter, with lower d-excess values implying a shallower
607 rooting depth (West et al. 2012, Simonin et al. 2014, Dawson & Simonin 2011, Dawson 1993).
608 Deuterium-excess values for red maple are generally lower than red oak (Figure 6). These values
609 were also lower than any of the environmental water sources sampled, likely due to evaporation
610 between soil infiltration and root uptake. In contrast, oak xylem water d-excess values overlap
611 with the values observed for local surface waters and for shallow ground water sampled from
612 wells (Figure 6). These results demonstrate that red maple predominantly uses shallow soil
613 waters, while red oak uses deeper soil waters.

614

615 *Whole-plant hydraulic strategy*

616 The proposed safety-efficiency tradeoff is typically discussed with respect to traits
617 existing within the same plant organ (i.e. xylem) (Manzoni et al. 2013, Gleason et al. 2016).
618 However, if we extend the theoretical concept to the emergent whole-plant hydraulic framework,
619 we could consider red oaks and maples within our research site as representations of opposing
620 ends of this spectrum. Red oaks did not exhibit the water stress that would be predicted from
621 their cavitation risk-prone xylem architecture and leaf hydraulic strategy. In fact, red maple, a
622 risk-adverse species, proved more sensitive to soil water content than oak (Figure 3, Figure 4).
623 Coupled with the xylem isotope analysis, these results indicate that during conditions typical to a
624 hydrologically regular year, the rooting strategy of red oaks offsets and may overcome the risks
625 associated with its leaf and xylem hydraulic traits. Due to deeper root-water uptake, red oaks are
626 able to maintain steady transpiration rates during dry periods. Red maples, which rely more on
627 ephemeral surficial soil waters and employ risk-adverse xylem and leaf traits, are unable to meet
628 the levels of Ψ_L required for maintaining high transpiration rates by the isohydric stomatal
629 strategy when soil moisture is low. Therefore, red maples close stomata in response to high VPD
630 and suffer depleted stem water storage in dry inter-storm periods.

631 Traits along each of the three axes of the whole-plant hydraulic strategy (i.e. leaf, stem,
632 and root) synergistically control stomatal conductance and thus both transpiration and
633 photosynthesis. Over a long timescale, these factors affect plant growth and survival. In our site,

634 the deep rooting strategy of red oaks increases the ability to endure short-term (days-weeks)
635 water stress without catastrophic loss of conductivity or reductions in growth. Red oaks
636 demonstrated no correlation between incremental annual bole growth and mean annual soil
637 moisture at 30 cm, while red maple displayed a strong correlation (Figure 7). Bole growth was
638 not correlated with mean growing season soil moisture, which may relate to the complex
639 climatological and ecological significance of the winter precipitation (Reinmann & Templer
640 2016) and to the uneven distribution of bole growth throughout the growing season (Jackson
641 1952). Nonetheless, our growth analysis results demonstrate that red maple growth responds to
642 soil water status at shallow depths, while oak growth does not. The carbon starvation hypothesis
643 posed by McDowell et al. (2008) states that anisohydric species are susceptible to extreme
644 drought due to hydraulic failure, while isohydric species will experience mortality during a
645 prolonged drought due to limitations on carbon uptake imposed by tight stomatal control. The
646 correlation between soil moisture and growth in the isohydric, but not the anisohydric species,
647 supports this hypothesis. The additional drought tolerance afforded to red oak through its rooting
648 strategy makes it less vulnerable to hydraulic failure than hypothesized on the basis of its
649 stomatal regulation strategy and xylem architecture. This result highlights the importance of a
650 synergistic, whole-tree approach to the study of tree hydrodynamics and their role in drought
651 mortality. Ecologically, the combination of deep or efficient roots, highly conductive hydraulic
652 tissues and anisohydric stomatal strategy may be important for drought tolerance particularly in
653 arid and semi-arid regions (Brooks et al. 2010, Miller et al. 2010). Shallow roots, isohydric
654 stomatal regulation, and less-conductive wood may be traits of species which are highly
655 competitive in relatively wet places and during periods of high surface soil moisture, while
656 avoiding stress when soil moisture availability is low.

657 Results from the sensitivity analysis demonstrated that traits at each organ level play a
658 defining role in shaping intra-daily transpiration dynamics, as well as the transpiration response
659 to drying soil (Figure 8). The diversity in the magnitude and the diurnal pattern generated by
660 each of the trait combinations affirms the importance of using a whole-plant framework to
661 characterize plant hydraulic strategy rather than a single axis. We emphasize that our sensitivity
662 analysis did not aim to reproduce our sap flux results, and there are similarities and differences
663 between observed sap flux and the transpiration sensitivity test simulations for the suites of traits
664 that match most closely with traits observed for red oak (simulation case #1) and red maple

665 (simulation case #8). Similarly to the measured oak sap flux during the mini-drought (Figure 3),
666 the simulated transpiration from case #1 (Figure 8) showed limited skewness towards the
667 morning hours and no decline across the 7-day simulation period. In contrast to the observed sap
668 flux data in which sap flux from maple exceeded that of oak during non-limiting soil conditions
669 (Figure 5), the magnitude of simulation case #1 consistently exceeded that of simulation case #8
670 (most similar to red maple, Figure 8) as well as that of case #4 (isohydric, diffuse porous, deep
671 roots, Figure 8) which could be considered analogous to a constantly well-watered maple. As in
672 the sap flux data recorded for maple, transpiration from simulation case #8 (Figure 8) declined
673 steadily with declining soil water availability to near zero with a distinct skew towards the
674 morning hours. Diurnal skewness is most pronounced during the least dry days of the simulation
675 (Day 1 and Day 2) and becomes increasing smaller as overall transpiration declines. Observed
676 sap flux, on the other hand, manifests the skew most strongly when the soil is driest (DOY 221
677 and 222, Figure 3).

678 This skewed shape of diurnal transpiration depends on the stomatal response to VPD as
679 well as the use of stem-stored water for transpiration early in the day, and is partially responsible
680 for the diurnal hysteresis of transpiration (Novick et al. 2014, Zhang et al. 2014, Matheny et al.
681 2014b). This hysteresis has been hypothesized to be the source of missed intra-daily dynamics of
682 latent heat flux as simulated by land-surface models (Matheny et al. 2014a). Current land-surface
683 models (LSMs) cluster species into plant functional types (PFTs), which characterize trees by
684 phenology, leaf traits, and bioclimatic limits, but do not explicitly represent hydraulic properties
685 (Matheny et al. 2016, Quillet et al. 2010, Yang et al. 2015). For example, red oaks and red
686 maples are often assigned to the same PFT (temperate deciduous broadleaf), despite their distinct
687 patterns of water acquisition and use. As such, these models are prone to mischaracterize
688 hydrologic cycling between the land surface and the atmosphere, and are unlikely to simulate
689 realistic ecosystem response to droughts, disturbances, or climate change (Link et al. 2014).
690 LSM representation of land-atmosphere water fluxes may be improved by replacing current PFT-
691 based parameterizations with new parameterizations that account for variability in whole-plant
692 hydraulic traits (Matheny et al. 2016). Alternatively, the incorporation of statistically scalable
693 tree-level hydrodynamics models (e. g. Sperry et al. 1998, Bohrer et al. 2005, Janott et al. 2011,
694 Gentine et al. 2015, Mirfenderesgi et al. 2016) into existing LSM schemes will permit leaf, stem,
695 and root level traits to be accounted for directly. The work of Xu et al. (2016) demonstrates this

696 pathway for model improvement. Although this method to incorporate plant hydraulic strategies
697 into LSMs will require increased model parameterization, tools such as the TRY Global Plant
698 Trait Database (Kattge et al. 2011) and frameworks of ecosystem level functional properties
699 (Musavi et al. 2015) will facilitate the effort.

700

701 **Conclusion**

702 The emergent phenotypical hydraulic traits at each of the root, stem, and leaf levels
703 combine to form a whole-plant hydraulic strategy. This strategy shapes inter- and intra-daily
704 patterns of water flux, which contribute to long-term patterns of growth and individual responses
705 to microclimate. The outcomes of these species-specific behaviors may remain unresolved by
706 current modeling frameworks due to the over-aggregation of hydraulically dissimilar species into
707 the same functional class. We therefore advocate the incorporation of more physically and
708 structurally realistic plant hydraulics sub-models into larger land-surface and ecosystem models.
709 These plant hydraulics models, such as FETCH2, will replace the current empirical link between
710 soil moisture and stomatal conductance with mechanistic representations of stomatal response to
711 stem, branch, or leaf water potential. Our results suggest that improving model parameterizations
712 in this manner will be critical for improving simulations of ecosystem responses to drought and
713 other changes to canopy structure, forest composition, and climate. Increased accuracy in model
714 representations of transpiration and the combination of traits that control it will translate directly
715 into better predictions of growth and mortality, as well as improved simulations of the terrestrial
716 surface energy budget and global carbon and water balances.

717

718 **Acknowledgements**

719 Funding for this study was provided by U.S. Department of Energy's Office of Science,
720 Office of Biological and Environmental Research, Terrestrial Ecosystem Sciences Program
721 Award No. DE-SC0007041, Ameriflux Management program under Flux Core Site Agreement
722 No. 7090915 through Lawrence Berkeley National Laboratory, and the National Science
723 Foundation Hydrological Science grant 1521238. Support for A.M.M. was provided by The Ohio
724 State University Presidential Fellowship and the P.E.O. Scholar Award. R.P.F. received support
725 from NSF Graduate Research Fellowship 2011094378. The authors have no conflicts of interest

726 to declare. Any opinions, findings, and conclusions or recommendations expressed in this
727 material are those of the authors and do not necessarily reflect the views of the funding agencies.

728

729 **References**

- 730 Abrams MD 1990. Adaptations and responses to drought in *Quercus* species of North America.
731 *Tree Physiol.* **7**, 227-238.
- 732 Allen MF 2009. Water relations in the mycorrhizosphere. In: Luttge U, Beyschlag W, Budel B,
733 Francis D (eds) *Progress in Botany*, pp 257-276. Springer-Verlag, Berlin & Heidelberg,
734 Germany.
- 735 Attia Z, Domec JC, Oren R, Way DA, Moshelion M 2015. Growth and physiological responses
736 of isohydric and anisohydric poplars to drought. *J. Exp. Bot.* DOI: 10.1093/jxb/erv195.
- 737 Baldocchi DD, Xu LK 2007. What limits evaporation from Mediterranean oak woodlands - The
738 supply of moisture in the soil, physiological control by plants or the demand by the
739 atmosphere? *Adv. Water Resour.* **30**, 2113-2122. DOI: 10.1016/j.advwatres.2006.06.013.
- 740 Barnes CJ, Allison GB 1988. Tracing of water movement in the unsaturated zone using stable
741 isotopes of hydrogen and oxygen. *J. Hydrol.* **100**, 143-176. DOI: 10.1016/0022-
742 1694(88)90184-9.
- 743 Barnes CJ, Turner JV 1998. Isotopic Exchange in Soil Water. In: McDonnell C, Kendall JJ (eds)
744 *Isotope Tracers in Catchment Hydrology*, pp 137-163. Elsevier, Amsterdam.
- 745 Bohrer G, Mourad H, Laursen TA, Drewry D, Avissar R, Poggi D, Oren R, Katul GG 2005.
746 Finite element tree crown hydrodynamics model (FETCH) using porous media flow within
747 branching elements: A new representation of tree hydrodynamics. *Water Resour. Res.* **41**.
748 DOI: 10.1029/2005wr004181.
- 749 Bovard BD, Curtis PS, Vogel CS, Su H-B, Schmid HP 2005. Environmental controls on sap flow
750 in a northern hardwood forest. *Tree Physiol.* **25**, 31-38.
- 751 Breecker DO, Sharp ZD, McFadden LD 2009. Seasonal bias in the formation and stable isotopic
752 composition of pedogenic carbonate in modern soils from central New Mexico, USA. *Geol.*
753 *Soc. Am. Bull.* **121**, 630-640. DOI: 10.1130/b26413.1.
- 754 Brooks RJ, Barnard HR, Coulombe R, McDonnell JJ 2010. Ecohydrologic separation of water
755 between trees and streams in a Mediterranean climate. *Nat. Geosci.* **3**, 100-104.
- 756 Canadell J, Jackson RB, Ehleringer JR, Mooney HA, Sala OE, Schulze ED 1996. Maximum
757 rooting depth of vegetation types at the global scale. *Oecologia* **108**, 583-595. DOI:
758 10.1007/bf00329030.
- 759 Canadell JG, Pataki DE, Pitelka L 2007. *Terrestrial ecosystems in a changing world*, Springer,
760 Berlin; New York.
- 761 Choat B, Jansen S, Brodribb TJ, Cochard H, Delzon S, Bhaskar R, Bucci SJ, Feild TS, Gleason
762 SM, Hacke UG, Jacobsen AL, Lens F, Maherali H, Martinez-Vilalta J, Mayr S, Mencuccini
763 M, Mitchell PJ, Nardini A, Pittermann J, Pratt RB, Sperry JS, Westoby M, Wright IJ, Zanne
764 AE 2012. Global convergence in the vulnerability of forests to drought. *Nature* **491**, 752-756.
765 DOI: 10.1038/nature11688.
- 766 Clearwater MJ, Meinzer FC, Andrade JL, Goldstein G, Holbrook NM 1999. Potential errors in
767 measurement of nonuniform sap flow using heat dissipation probes. *Tree Physiol.* **19**, 681-
768 687.

769 Cochard H, Breda N, Granier A, Aussenac G 1992. Vulnerability to air-embolism of 3 European
770 oak species (*Quercus petraea* (Matt) Liebl, *Q pubescens* Willd, *Q robur* L). *Ann. Sci. For.*
771 **49**, 225-233. DOI: 10.1051/forest:19920302.

772 Coplen TB 1996. New guidelines for reporting stable hydrogen, carbon, and oxygen isotope-
773 ratio data. *Geochim. Cosmochim. Acta* **60**, 3359-3360. DOI: [http://dx.doi.org/10.1016/0016-7037\(96\)00263-3](http://dx.doi.org/10.1016/0016-7037(96)00263-3).

774
775 Craig H 1961. Standard for reporting concentrations of deuterium and oxygen-18 in natural
776 waters. *Science* **133**, 1833-&. DOI: 10.1126/science.133.3467.1833.

777 Dansgaard W 1964. Stable isotopes in precipitation. *Tellus* **16**, 436-468.

778 Dawson TE 1993. Hydraulic lift and water use by plants: implications for water-balance,
779 performance and plant-plant interactions. *Oecologia* **95**, 565-574.

780 Dawson TE 1996. Determining water use by trees and forests from isotopic, energy balance and
781 transpiration analyses: the roles of tree size and hydraulic lift. *Tree Physiol.* **16**, 263-272.

782 Dawson TE, Simonin KA 2011. The roles of stable isotopes in forest hydrology and
783 biogeochemistry. In: Levia DF, Carlyle-Moses D, Tanaka T (eds) *Forest Hydrology and*
784 *Biogeochemistry*, pp 137-161. Springer Netherlands.

785 Ehleringer JR, Dawson TE 1992. Water uptake by plants - perspectives from stable isotope
786 composition. *Plant Cell Environ.* **15**, 1073-1082. DOI: 10.1111/j.1365-3040.1992.tb01657.x.

787 Ford CR, Hubbard RM, Vose JM 2011. Quantifying structural and physiological controls on
788 variation in canopy transpiration among planted pine and hardwood species in the southern
789 Appalachians. *Ecohydrol.* **4**, 183-195. DOI: 10.1002/eco.136.

790 Friedman I, Harris JM, Smith GI, Johnson CA 2002. Stable isotope composition of waters in the
791 Great Basin, United States - 1. Air-mass trajectories. *J. Geophys. Res.-Atmos.* **107**, 14. DOI:
792 10.1029/2001jd000565.

793 Gaines KP, Stanley JW, Meinzer FC, McCulloh KA, Woodruff DR, Chen W, Adams TS, Lin
794 HS, Eissenstat DM 2015. Reliance on shallow soil water in a mixed-hardwood forest in
795 central Pennsylvania. *Tree Physiol.* DOI: 10.1093/treephys/tpv113.

796 Gao JG, Zhao P, Shen WJ, Niu JF, Zhu LW, Ni GY 2015. Biophysical limits to responses of
797 water flux to vapor pressure deficit in seven tree species with contrasting land use regimes.
798 *Agric. For. Meteorol.* **200**, 258-269. DOI: 10.1016/j.agrformet.2014.10.007.

799 Gat JR 1996. Oxygen and hydrogen isotopes in the hydrologic cycle. *Annu. Rev. Earth Planet.*
800 *Sci.* **24**, 225-262. DOI: 10.1146/annurev.earth.24.1.225.

801 Gazis C, Feng XH 2004. A stable isotope study of soil water: evidence for mixing and
802 preferential flow paths. *Geoderma* **119**, 97-111. DOI: 10.1016/s0016-7061(03)00243-x.

803 Gentile P, Guérin M, Uriarte M, McDowell NG, Pockman WT 2015. An allometry-based model
804 of the survival strategies of hydraulic failure and carbon starvation. *Ecohydrol.* DOI:
805 10.1002/eco.1654.

806 Gleason SM, Westoby M, Jansen S, Choat B, Hacke UG, Pratt RB, Bhaskar R, Brodrribb TJ,
807 Bucci SI, Cao KF, Cochard H, Delzon S, Domec JC, Fan ZX, Feild TS, Jacobsen AL,
808 Johnson DM, Lens F, Maherali H, Martinez-Vilalta J, Mayr S, McCulloh KA, Mencuccini
809 M, Mitchell PJ, Morris H, Nardini A, Pittermann J, Plavcova L, Schreiber SG, Sperry JS,
810 Wright IJ, Zanne AE 2016. Weak tradeoff between xylem safety and xylem-specific
811 hydraulic efficiency across the world's woody plant species. *New Phytol.* **209**, 123-136. DOI:
812 10.1111/nph.13646.

813 Gough CM, Curtis PS 1999-. AmeriFlux US_UMB University of Michigan Biological Station
814 Dataset. DOI: 10.17190/AMF/1246107.

815 Gough CM, Hardiman BS, Nave LE, Bohrer G, Maurer KD, Vogel CS, Nadelhoffer KJ, Curtis
816 PS 2013. Sustained carbon uptake and storage following moderate disturbance in a Great
817 Lakes forest. *Ecol. Appl.* **23**, 1202-1215. DOI: 10.1890/12-1554.1.

818 Gough CM, Vogel CS, Hardiman B, Curtis PS 2010. Wood net primary production resilience in
819 an unmanaged forest transitioning from early to middle succession. *For. Ecol. Manage.* **260**,
820 36-41. DOI: 10.1016/j.foreco.2010.03.027.

821 Granier A 1985. A new method of sap flow measurement in tree stems. *Ann. Sci. For.* **42**, 193-
822 200. DOI: 10.1051/forest:19850204.

823 Granier A 1987. Evaluation of transpiration in a Douglas-Fir stand by means of sap flow
824 measurements. *Tree Physiol.* **3**, 309-319.

825 Gu L, Pallardy SG, Hosman KP, Sun Y 2015. Drought-influenced mortality of tree species with
826 different predawn leaf water dynamics in a decade-long study of a central US forest.
827 *Biogeosciences* **12**, 2831-2845. DOI: 10.5194/bg-12-2831-2015.

828 He LL, Ivanov VY, Bohrer G, Thomsen JE, Vogel CS, Moghaddam M 2013. Temporal
829 dynamics of soil moisture in a northern temperate mixed successional forest after a
830 prescribed intermediate disturbance. *Agric. For. Meteorol.* **180**, 22-33. DOI:
831 10.1016/j.agrformet.2013.04.014.

832 Hernandez-Jantana V, Martinez-Fernandez J, Moran C, Cano A 2008. Response of *Quercus*
833 *pyrenaica* (melojo oak) to soil water deficit: a case study in Spain. *Eur. J. For. Res.* **127**,
834 369-376. DOI: 10.1007/s10342-008-0214-x.

835 Horton R, Hart SC 1998. Hydraulic lift: a potentially important ecosystem process. *Trends Ecol.*
836 *Evol.* **13**, 232-235. DOI: 10.1016/s0169-5347(98)01328-7.

837 Jackson LWR 1952. Radial growth of forest trees in the Georgia piedmont. *Ecology* **33**, 336-341.
838 DOI: 10.2307/1932829.

839 Jackson RB, Canadell J, Ehleringer JR, Mooney HA, Sala OE, Schulze ED 1996. A global
840 analysis of root distributions for terrestrial biomes. *Oecologia* **108**, 389-411. DOI: Doi
841 10.1007/Bf00333714.

842 Janott M, Gayler S, Gessler A, Javaux M, Klier C, Priesack E 2011. A one-dimensional model of
843 water flow in soil-plant systems based on plant architecture. *Plant Soil* **341**, 233-256. DOI:
844 10.1007/s11104-010-0639-0.

845 Kattge J, Diaz S, Lavorel S, Prentice C, Leadley P, Bonisch G, Garnier E, Westoby M, Reich
846 PB, Wright IJ, Cornelissen JHC, Violle C, Harrison SP, van Bodegom PM, Reichstein M,
847 Enquist BJ, Soudzilovskaia NA, Ackerly DD, Anand M, Atkin O, Bahn M, Baker TR,
848 Baldocchi D, Bekker R, Blanco CC, Blonder B, Bond WJ, Bradstock R, Bunker DE,
849 Casanoves F, Cavender-Bares J, Chambers JQ, Chapin FS, Chave J, Coomes D, Cornwell
850 WJ, Craine JM, Dobrin BH, Duarte L, Durka W, Elser J, Esser G, Estiarte M, Fagan WF,
851 Fang J, Fernandez-Mendez F, Fidelis A, Finegan B, Flores O, Ford H, Frank D, Freschet GT,
852 Fyllas NM, Gallagher RV, Green WA, Gutierrez AG, Hickler T, Higgins SI, Hodgson JG,
853 Jalili A, Jansen S, Joly CA, Kerkhoff AJ, Kirkup D, Kitajima K, Kleyer M, Klotz S, Knops
854 JMH, Kramer K, Kuhn I, Kurokawa H, Laughlin D, Lee TD, Leishman M, Lens F, Lenz T,
855 Lewis SL, Lloyd J, Llusia J, Louault F, Ma S, Mahecha MD, Manning P, Massad T, Medlyn
856 BE, Messier J, Moles AT, Muller SC, Nadrowski K, Naeem S, Niinemets U, Nollert S,
857 Nuske A, Ogaya R, Oleksyn J, Onipchenko VG, Onoda Y, Ordonez J, Overbeck G, Ozinga
858 WA, Patino S, Paula S, Pausas JG, Penuelas J, Phillips OL, Pillar V, Poorter H, Poorter L,
859 Poschlod P, Prinzing A, Proulx R, Rammig A, Reinsch S, Reu B, Sack L, Salgado-Negre B,
860 Sardans J, Shiodera S, Shipley B, Siefert A, Sosinski E, Soussana JF, Swaine E, Swenson N,

861 Thompson K, Thornton P, Waldram M, Weiher E, White M, White S, Wright SJ, Yguel B,
862 Zaehle S, Zanne AE, Wirth C 2011. TRY - a global database of plant traits. *Glob. Change*
863 *Biol.* **17**, 2905-2935. DOI: 10.1111/j.1365-2486.2011.02451.x.

864 Kocher P, Horna V, Leuschner C 2013. Stem water storage in five coexisting temperate broad-
865 leaved tree species: significance, temporal dynamics and dependence on tree functional traits.
866 *Tree Physiol.* **33**, 817-832. DOI: 10.1093/treephys/tpt055.

867 Link P, Simonin K, Maness H, Oshun J, Dawson T, Fung I 2014. Species differences in the
868 seasonality of evergreen tree transpiration in a Mediterranean climate: Analysis of multiyear,
869 half-hourly sap flow observations. *Water Resour. Res.* **50**, 1869-1894. DOI:
870 10.1002/2013wr014023.

871 Maherali H, Moura CF, Caldeira MC, Willson CJ, Jackson RB 2006. Functional coordination
872 between leaf gas exchange and vulnerability to xylem cavitation in temperate forest trees.
873 *Plant Cell Environ.* **29**, 571-583. DOI: 10.1111/j.1365-3040.2005.01433.x.

874 Manzoni S 2014. Integrating plant hydraulics and gas exchange along the drought-response trait
875 spectrum. *Tree Physiol.* **34**, 1031-1034. DOI: 10.1093/treephys/tpu088.

876 Manzoni S, Vico G, Katul G, Palmroth S, Porporato A 2014. Optimal plant water-use strategies
877 under stochastic rainfall. *Water Resour. Res.* **50**, 5379-5394. DOI: 10.1002/2014WR015375.

878 Manzoni S, Vico G, Katul GG, Palmroth S, Jackson RB, Porporato A 2013. Hydraulic limits on
879 maximum plant transpiration and the emergence of the safety-efficiency trade-off. *New*
880 *Phytol.* DOI: 10.1111/nph.12126.

881 Martínez-Vilalta J, Poyatos R, Aguade D, Retana J, Mencuccini M 2014. A new look at water
882 transport regulation in plants. *New Phytol.* **204**, 105-115. DOI: 10.1111/nph.12912.

883 Matherly AM, Bohrer G, Garrity SR, Morin TH, Howard CJ, Vogel CS 2015. Observations of
884 stem water storage in trees of opposing hydraulic strategies. *Ecosphere* **6**, 165. DOI:
885 <http://dx.doi.org/10.1890/ES15-00170.1>.

886 Matherly AM, Bohrer G, Stoy PC, Baker I, Black AT, Desai AR, Dietze M, Gough CM, Ivanov
887 VY, Jassal R, Novick K, Schäfer K, Verbeeck H 2014a. Characterizing the diurnal patterns
888 of errors in the prediction of evapotranspiration by several land-surface models: an NACP
889 analysis. *J. Geophys. Res.* **119**, 1458-1473. DOI: 10.1002/2014JG002623.

890 Matherly AM, Bohrer G, Vogel CS, Morin TH, He L, Frasson RPM, Mirfenderesgi G, Schäfer
891 KVK, Gough CM, Ivanov VY, Curtis PS 2014b. Species-specific transpiration responses to
892 intermediate disturbance in a northern hardwood forest. *J. Geophys. Res.* **119**, 2292-2311.
893 DOI: 10.1002/2014JG002804.

894 Matherly AM, Mirfenderesgi G, Bohrer G 2016. Trait-based representation of hydrological
895 functional properties of plants in weather and ecosystem models. *Plant Diversity* **In press**.

896 Matthes JH, Goring S, Williams JW, Dietze MC 2016. Benchmarking historical CMIP5 plant
897 functional types across the Upper Midwest and Northeastern United States. *J. Geophys. Res.*,
898 2015JG003175. DOI: 10.1002/2015JG003175.

899 Maurer KD, Hardiman BS, Vogel CS, Bohrer G 2013. Canopy-structure effects on surface
900 roughness parameters: Observations in a Great Lakes mixed-deciduous forest. *Agric. For.*
901 *Meteorol.* **177**, 24-34. DOI: 10.1016/j.agrformet.2013.04.002.

902 McCulloh KA, Johnson DM, Meinzer FC, Voelker SL, Lachenbruch B, Domec J-C 2012.
903 Hydraulic architecture of two species differing in wood density: opposing strategies in co-
904 occurring tropical pioneer trees. *Plant Cell Environ.* **35**, 116-125. DOI: 10.1111/j.1365-
905 3040.2011.02421.x.

906 McDowell N, Pockman WT, Allen CD, Breshears DD, Cobb N, Kolb T, Plaut J, Sperry JS, West
907 A, Williams DG, Yezpe EA 2008. Mechanisms of plant survival and mortality during
908 drought: why do some plants survive while others succumb to drought? *New Phytol.* **178**,
909 719-739. DOI: 10.1111/j.1469-8137.2008.02436.x.

910 Meinzer FC, Andrade JL, Goldstein G, Holbrook NM, Cavelier J, Wright SJ 1999. Partitioning
911 of soil water among canopy trees in a seasonally dry tropical forest. *Oecologia* **121**, 293-301.
912 DOI: 10.1007/s004420050931.

913 Meinzer FC, McCulloh KA, Lachenbruch B, Woodruff DR, Johnson DM 2010. The blind men
914 and the elephant: the impact of context and scale in evaluating conflicts between plant
915 hydraulic safety and efficiency. *Oecologia* **164**, 287-296. DOI: 10.1007/s00442-010-1734-x.

916 Meinzer FC, Woodruff DR, Eissenstat DM, Lin HS, Adams TS, McCulloh KA 2013. Above-
917 and belowground controls on water use by trees of different wood types in an eastern US
918 deciduous forest. *Tree Physiol.* **33**, 345-356. DOI: 10.1093/treephys/tpt012.

919 Meinzer FC, Woodruff DR, Marias DE, McCulloh KA, Sevanto S 2014. Dynamics of leaf water
920 relations components in co-occurring iso- and anisohydric conifer species. *Plant Cell*
921 *Environ* **37**, 2577-2586. DOI: 10.1111/pce.12327.

922 Miller GR, Chen XY, Rubin Y, Ma SY, Baldocchi DD 2010. Groundwater uptake by woody
923 vegetation in a semiarid oak savanna. *Water Resour. Res.* **46**, 14. DOI:
924 10.1029/2009wr008902.

925 Mirfenderesgi G, Bohrer G, Matheny AM, Fatichi S, Frasson RPM, Schäfer KVR 2016. Tree-
926 level hydrodynamic approach for modeling aboveground water storage and stomatal
927 conductance illuminates the effects of tree hydraulic strategy. *J. Geophys. Res.* **In press**.

928 Musavi T, Mahecha MD, Migliavacca M, Reichstein M, van de Weg MJ, van Bodegom PM,
929 Bahn M, Wirth C, Reich PB, Schrodt F, Kattge J 2015. The imprint of plants on ecosystem
930 functioning: A data-driven approach. *International Journal of Applied Earth Observation*
931 *and Geoinformation* **43**, 119-131. DOI: 10.1016/j.jag.2015.05.009.

932 Nadezhkina N, Ferreira MI, Silva R, Pacheco CA 2008. Seasonal variation of water uptake of a
933 *Quercus suber* tree in Central Portugal. *Plant Soil* **305**, 105-119. DOI: 10.1007/s11104-007-
934 9398-y.

935 Nave LL, Gough CM, Maurer KD, Bohrer G, Hardiman BS, Le Moine J, Munoz AB,
936 Nadelmeffer KJ, Sparks JP, Strahm BD, Vogel CS, Curtis PS 2011. Disturbance and the
937 resilience of coupled carbon and nitrogen cycling in a north temperate forest. *J. Geophys.*
938 *Res.* **116**. DOI: 10.1029/2011jg001758.

939 Nolf M, Creek D, Duursma R, Holtum J, Mayr S, Choat B 2015. Stem and leaf hydraulic
940 properties are finely coordinated in three tropical rainforest tree species. *Plant Cell Environ.*
941 DOI: 10.1111/pce.12581.

942 Novick K, Brantley S, Miniati CF, Walker J, Vose JM 2014. Inferring the contribution of
943 advection to total ecosystem scalar fluxes over a tall forest in complex terrain. *Agric. For.*
944 *Meteorol.* **185**, 1-13. DOI: 10.1016/j.agrformet.2013.10.010.

945 Novick KA, Miniati CF, Vose JM 2015. Drought limitations to leaf-level gas exchange: results
946 from a model linking stomatal optimization and cohesion tension theory. *Plant Cell Environ.*
947 DOI: 10.1111/pce.12657.

948 Oishi AC, Oren R, Stoy PC 2008. Estimating components of forest evapotranspiration: A
949 footprint approach for scaling sap flux measurements. *Agric. For. Meteorol.* **148**, 1719-1732.
950 DOI: 10.1016/j.agrformet.2008.06.013.

- 951 Oren R, Pataki DE 2001. Transpiration in response to variation in microclimate and soil moisture
952 in southeastern deciduous forests. *Oecologia* **127**, 549-559. DOI: 10.1007/s004420000622.
- 953 Phillips SL, Ehleringer JR 1995. Limited uptake of summer precipitation by bigtooth maple
954 (*Acer grandidentatum* Nutt) and Gambel's oak (*Quercus gambelii* Nutt). *Trees* **9**, 214-219.
955 DOI: 10.1007/bf00195275.
- 956 Pinto CA, Nadezhdina N, David JS, Kurz-Besson C, Caldeira MC, Henriques MO, Monteiro FG,
957 Pereira JS, David TS 2014. Transpiration in *Quercus suber* trees under shallow water table
958 conditions: the role of soil and groundwater. *Hydrol. Process.* **28**, 6067-6079. DOI:
959 10.1002/hyp.10097.
- 960 Pockman WT, Sperry JS 2000. Vulnerability to xylem cavitation and the distribution of Sonoran
961 desert vegetation. *Am. J. Bot.* **87**, 1287-1299. DOI: 10.2307/2656722.
- 962 Poulter B, Clais P, Hodson E, Lischke H, Maignan F, Plummer S, Zimmermann NE 2011. Plant
963 functional type mapping for earth system models. *Geosci. Model Dev.* **4**, 993-1010. DOI:
964 10.5197/gmd-4-993-2011.
- 965 Quillet A, Peng CH, Garneau M 2010. Toward dynamic global vegetation models for simulating
966 vegetation-climate interactions and feedbacks: recent developments, limitations, and future
967 challenges. *Environmental Reviews* **18**, 333-353. DOI: 10.1139/a10-016.
- 968 Rawls WJ, Brakensiek DL, Saxton KE 1982. Estimation of soil water properties. *Trans. ASAE*
969 **25**, 1316-1328.
- 970 Reinmann AB, Templer PH 2016. Reduced winter snowpack and greater soil frost reduce live
971 root biomass and stimulate radial growth and stem respiration of red maple (*Acer rubrum*)
972 trees in a mixed-hardwood forest. *Ecosystems* **19**, 129-141. DOI: 10.1007/s10021-015-9923-
973 4.
- 974 Roman DT, Novick KA, Brzostek ER, Dragoni D, Rahman F, Phillips RP 2015. The role of
975 isohydric and anisohydric species in determining ecosystem-scale response to severe
976 drought. *Oecologia*, 1-14. DOI: 10.1007/s00442-015-3380-9.
- 977 Scholl MA, Ingebritsen SE, Janik CJ, Kauhikaua JP 1996. Use of precipitation and groundwater
978 isotopes to interpret regional hydrology on a tropical volcanic island: Kilauea volcano area,
979 Hawaii. *Water Resour. Res.* **32**, 3525-3537. DOI: 10.1029/95wr02837.
- 980 Simonin KA, Link P, Rempe D, Miller S, Oshun J, Bode C, Dietrich WE, Fung I, Dawson TE
981 2014. Vegetation induced changes in the stable isotope composition of near surface humidity.
982 *Ecophysiol.* **7**, 936-949. DOI: 10.1002/eco.1420.
- 983 Skelton RP, West AG, Dawson TE 2015. Predicting plant vulnerability to drought in biodiverse
984 regions using functional traits. *Proceedings of the National Academy of Sciences* **112**, 5744-
985 5749. DOI: 10.1073/pnas.1503376112.
- 986 Sperry JS, Adler FR, Campbell GS, Comstock JP 1998. Limitation of plant water use by
987 rhizosphere and xylem conductance: results from a model. *Plant Cell Environ.* **21**, 347-359.
988 DOI: 10.1046/j.1365-3040.1998.00287.x.
- 989 Sperry JS, Nichols KL, Sullivan JEM, Eastlack SE 1994. Xylem embolism in ring-porous,
990 diffuse-porous and coniferous trees of northern Utah and interior Alaska. *Ecology* **75**, 1736-
991 1752. DOI: 10.2307/1939633.
- 992 Thomsen J, Bohrer G, Matheny AM, Ivanov VY, He L, Renninger H, Schäfer K 2013.
993 Contrasting hydraulic strategies during dry soil conditions in *Quercus rubra* and *Acer*
994 *rubrum* in a sandy site in Michigan. *Forests* **4**, 1106-1120.
- 995 Tognetti R, Longobucco A, Raschi A 1998. Vulnerability of xylem to embolism in relation to
996 plant hydraulic resistance in *Quercus pubescens* and *Quercus ilex* co-occurring in a

997 Mediterranean coppice stand in central Italy. *New Phytol.* **139**, 437-447. DOI:
998 10.1046/j.1469-8137.1998.00207.x.
999 Van Genuchten MT 1980. A closed form equation for predicting the hydraulic conductivity of
1000 unsaturated soils. *Soil Sci. Soc. Am. J.* **44**, 892-898.
1001 von Allmen EI, Sperry JS, Bush SE 2014. Contrasting whole-tree water use, hydraulics, and
1002 growth in a co-dominant diffuse-porous vs. ring-porous species pair. *Trees*, 1-12. DOI:
1003 10.1007/s00468-014-1149-0.
1004 West AG, Dawson TE, February EC, Midgley GF, Bond WJ, Aston TL 2012. Diverse functional
1005 responses to drought in a Mediterranean-type shrubland in South Africa. *New Phytol.* **195**,
1006 396-407. DOI: 10.1111/j.1469-8137.2012.04170.x.
1007 West AG, Goldsmith GR, Matimati I, Dawson TE 2011. Spectral analysis software improves
1008 confidence in plant and soil water stable isotope analyses performed by isotope ratio infrared
1009 spectroscopy (IRIS). *Rapid Commun. Mass Spectrom.* **25**, 2268-2274. DOI:
1010 10.1002/rcm.5126.
1011 Wullschlegel SD, Hanson PJ, Todd DE 1996. Measuring stem water content in four deciduous
1012 hardwoods with a time-domain reflectometer. *Tree Physiol.* **16**, 809-815.
1013 Wullschlegel SD, Meinzer FC, Vertessy RA 1998. A review of whole-plant water use studies in
1014 trees. *Tree Physiol.* **18**, 499-512.
1015 Xu X, Medvigy D, Powers JS, Becknell JM, Guan K 2016. Diversity in plant hydraulic traits
1016 explains seasonal and inter-annual variations of vegetation dynamics in seasonally dry
1017 tropical forests. *New Phytol.* DOI: 10.1111/nph.14009.
1018 Yang YZ, Zhu QA, Peng CH, Wang H, Chen H 2015. From plant functional types to plant
1019 functional traits: A new paradigm in modelling global vegetation dynamics. *Progress in*
1020 *Physical Geography* **39**, 514-535. DOI: 10.1177/0309133315582018.
1021 Zhang Q, Manzoni S, Katul GG, Porporato A, Yang D 2014. The hysteretic evapotranspiration—
1022 vapor pressure deficit relation. *J. Geophys. Res.* **119**, 125-140. DOI: 10.1002/2013JG002484.
1023

Author Manuscript

Table 1: Numbers and size ranges of sample trees used for each group of tree measurements.

<i>Sap flux</i>	<i>Red maple</i>	<i>Red Oak</i>
Measurement dates: 1 May – 31 September 2014		
Number of individuals	8	10
DBH range (cm)	11.9-22.3	21.7-37.2
<i>Stem water storage</i>		
Measurement dates: 10 July -14 September 2014		
Number of individuals	1	1
DBH (cm)	21.3	29.6
<i>Leaf level measurements</i>		
Measurement dates: 23 June – 12 July 2014		
Number of individuals	3	3
DBH range (cm)	19.2-28.7	24.0-33.5
<i>Xylem cores</i>		
Measurement dates: 29 June, 9-13 July, 4-8 August 2014		
Number of individuals	5	5
DBH range (cm)	22.8-37.2	33.5-47.9
<i>Growth measurements</i>		
Measurement dates: annually from 2001-2014		
Number of individuals	423	114
DBH range (cm)	8.2-40.6	9.5-58.5

1024

1025

1026

1027

Table 2: Trait values and references for parameters used to test FETCH2 sensitivity to leaf and stem level traits. Risk prone strategies indicate anisohydry or ring porous xylem. Risk adverse strategies represent isohydry or diffuse porous xylem.

Organ	Trait	Risk prone	Risk adverse	Reference
Leaf	C_3	4 (unitless)	7 (unitless)	Approx. from Thomsen et al. (2013)
	Φ_{σ}	-2.5 MPa	-1.2 MPa	Approx. from Thomsen et al. (2013)
Stem	Φ_0	-2.5 MPa	-2.0 MPa	(Mirfenderesgi et al. 2016)
	Φ_{88}	-0.5 MPa	-0.3 MPa	(Mirfenderesgi et al. 2016)
	K_{max}	1.33 kg m ⁻¹ s ⁻¹ MPa	0.55 kg m ⁻¹ s ⁻¹ MPa	(Maherali et al. 2006)
	C_l	-1.99 MPa	-2.58 MPa	Calc. from Choat et al. (2012)
	C_s	1.71 (unitless)	1.35 (unitless)	Calc. from Choat et al. (2012)

1028

1029

1030

1031

Author Manuscript

Table 3: Seasonal mean soil moisture (θ , m^3m^{-3}) and standard deviations for each measurement depth. Linear regression statistics for the relationship between residual sap flux and all seven soil moisture measurement depths between 5 and 300 cm. Residual sap flux is the residual generated by a linear regression of sap flux (dependent variable) and PAR and VPD and Ψ_s (independent variables). Significant values are indicated with an asterisk, the most significant relationship for each species is indicated by a double asterisk.

Depth	Mean seasonal θ m^3m^{-3}	Red maple		Red Oak	
		P values	R^2	P values	R^2
5 cm	0.086 ± 0.024	0.1812	0.0202	0.7638	0.0010
15 cm	0.109 ± 0.027	0.0001*	0.1614	0.4075	0.0078
30 cm	0.101 ± 0.021	8.9E-6**	0.2019	0.3045	0.0120
60 cm	0.083 ± 0.018	0.0003*	0.1360	0.2756	0.0135
100 cm	0.076 ± 0.018	0.0002*	0.1507	0.3231	0.0111
200 cm	0.043 ± 0.002	0.1590	0.0224	0.9534	0.0000
300 cm	0.044 ± 0.004	0.0009*	0.1190	0.0272**	0.0542

1034 **Figure Captions:**

Figure 1: Schematic diagram of risk levels associated with hydraulic strategy at each of the three levels of plant hydraulic control.

1035

Figure 2: Characterization of the different hydraulic traits: (A) Isohydic and anisohydric responses of stomatal conductance (β) as a function of leaf water potential. Weibull-shaped response curves are defined by C_3 and Φ_6 as given for anisohydry (value 1) and isohydry (value 2) in Table 2. (B) Response of relative xylem water content (RWC) to stem water potential as approximated for ring (left) and diffuse porous (right) trees. Curve shapes are defined by Φ_{50} and Φ_{88} for ring porous (value 1) and diffuse porous (value 2) as listed in Table 2. (C) Xylem conductivity for ring and diffuse porous species as constructed using values for red oak and red maple from Choat et al. (2012). Curve shapes are defined by parameters C_1 and C_2 as listed for ring (value 1) and diffuse porous (value 2) species in Table 2. (D) Water potential at the top of the root system (bottom-of-stem boundary condition) during a week-long dry-down event, as prescribed for cases having deep and shallow roots.

1036

Figure 3: Precipitation (mm) and soil water content ($\text{m}^3 \text{m}^{-3}$) integrated across the 3 m soil column (A), mean sap flux ($\text{g m}^{-2}\text{s}^{-1}$) for red oak ($n = 10$) and red maple ($n = 8$) trees (B), and stem water storage (kg) (C) for day of year 191-260 2014. The 2-week period of an inter-storm dry-down, or "mini-drought" (DOY 211-224), is marked by dashed vertical lines.

1037

Figure 4: Relationships between leaf water potential (Ψ_L , MPa) and vapor pressure deficit (VPD, kPa) at three times during the day for each species. Red oak leaf water potential was correlated with VPD at noon (13:30) (panel D, $P = 0.0040$, $R^2 = 0.46$) and in the afternoon (16:00) (panel F, $P = 0.0117$, $R^2 = 0.32$). Leaf water potential of red maple was weakly correlated to VPD in the afternoon (16:00) (panel E, $P = 0.0335$, $R^2 = 0.21$), but uncorrelated at dawn and noon.

1038

Figure 5: Isotopic compositions (δD vs $\delta^{18}O$) of xylem from red oak (A) and red maple (B) samples and environmental water samples (C). Isotopic compositions are reported as per mil deviations from the Vienna Standard Mean Ocean Water (VSMOW) standard. Error bars denote one standard error. Well waters were collected in August only. Samples that were collected in multiple months are color-coded by month. In all panels, the solid black line is the global meteoric water line, which describes the global relationship between δD and $\delta^{18}O$ in precipitation (Craig 1961). Maple xylem compositions (B) vary more than oak xylem (A) compositions throughout the collection period, indicating that the water sources used by maples are more isotopically variable than those used by oaks.

Figure 6: Deuterium excess for environmental and xylem water samples. The isotopic ranges observed in environmental water sources that were measured throughout the summer are shown as gray bars. Increasingly negative deuterium excess indicates that more evaporation has occurred. Samples having more evaporated isotopic signatures are associated with shallower water sources. Monthly means are presented by large black diamonds. Error bars on individual points are standard error (grey), and are the standard deviation of the distribution (black).

Figure 7: Mean annual bole growth (%) for years 2001-2014 for red oak (dots) and red maple (diamonds) as a function of soil moisture at 30 cm depth ($m^3 m^{-3}$). Bole growth of red maple was strongly correlated with mean annual soil moisture ($P = 0.0243$, $R^2 = 0.36$), while bole growth in red oak was not correlated to mean annual soil moisture ($P = 0.08$).

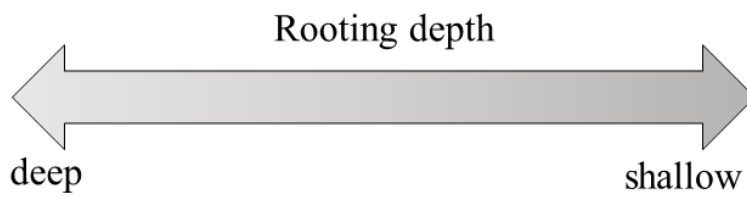
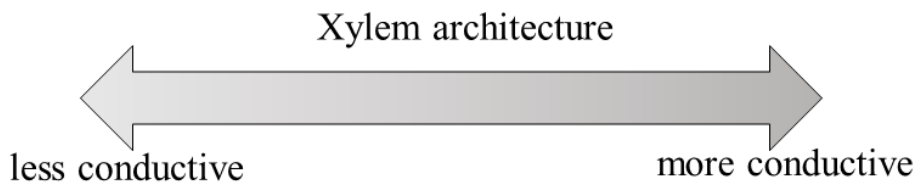
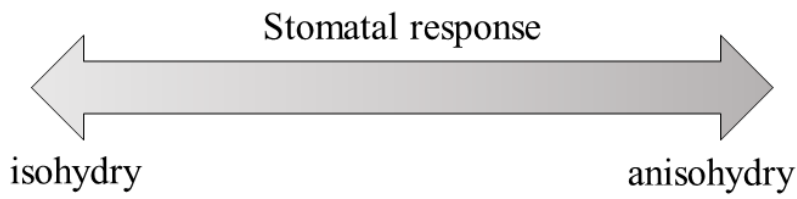
Figure 8: Sensitivity of simulated FETCH2 transpiration to different combinations of emergent leaf trait (isohydric or anisohydric) and xylem structure (ring or diffuse porous) assuming steady access to high (less negative) soil water potential afforded through a deep rooting strategy (dotted lines) or a shallow rooting strategy (solid lines). The shallow rooting strategy is described by steadily declining soil water potential (from -0.033 MPa on Day 1 to -1.5 MPa on Day 7).

ript

Axes of hydraulic control

Less cavitation risk

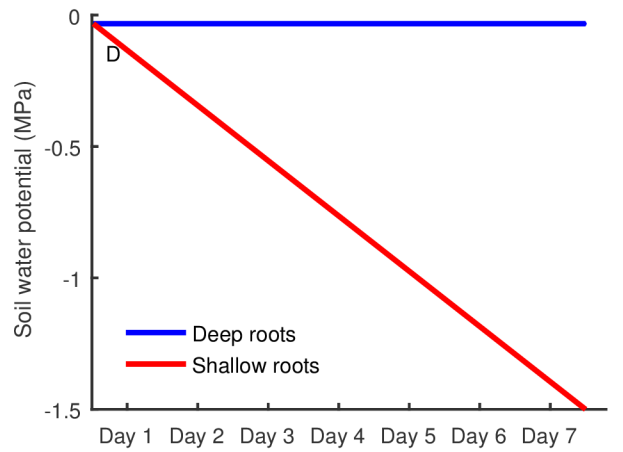
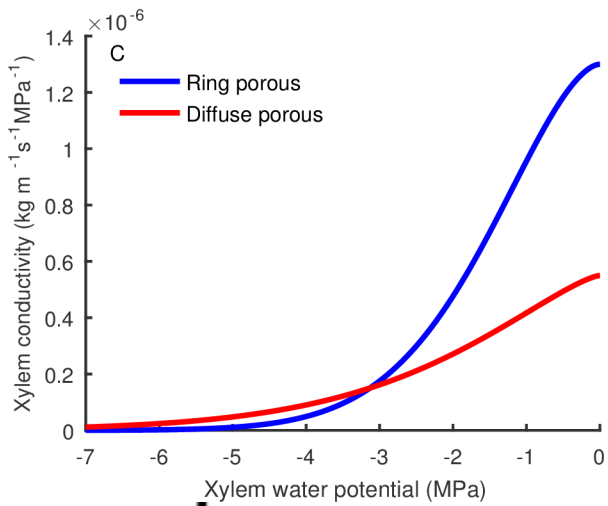
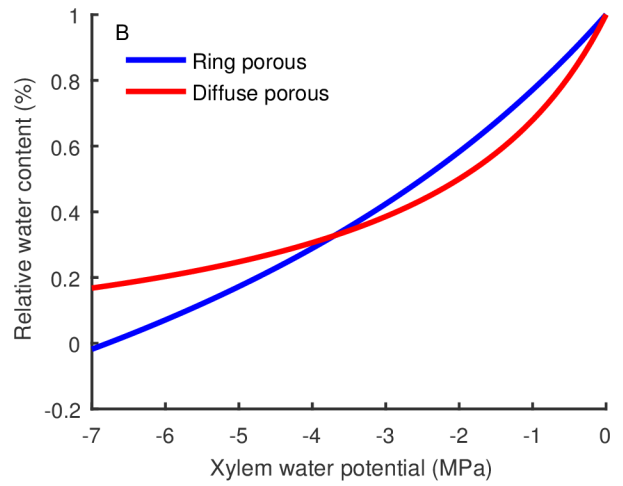
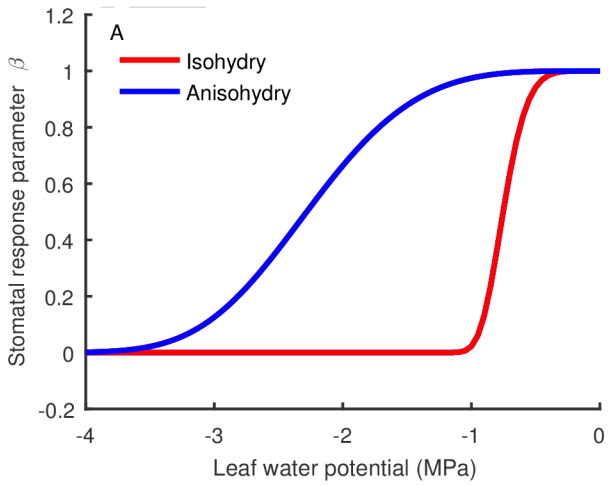
More cavitation risk



Aut

ECO_1815_F1.tif

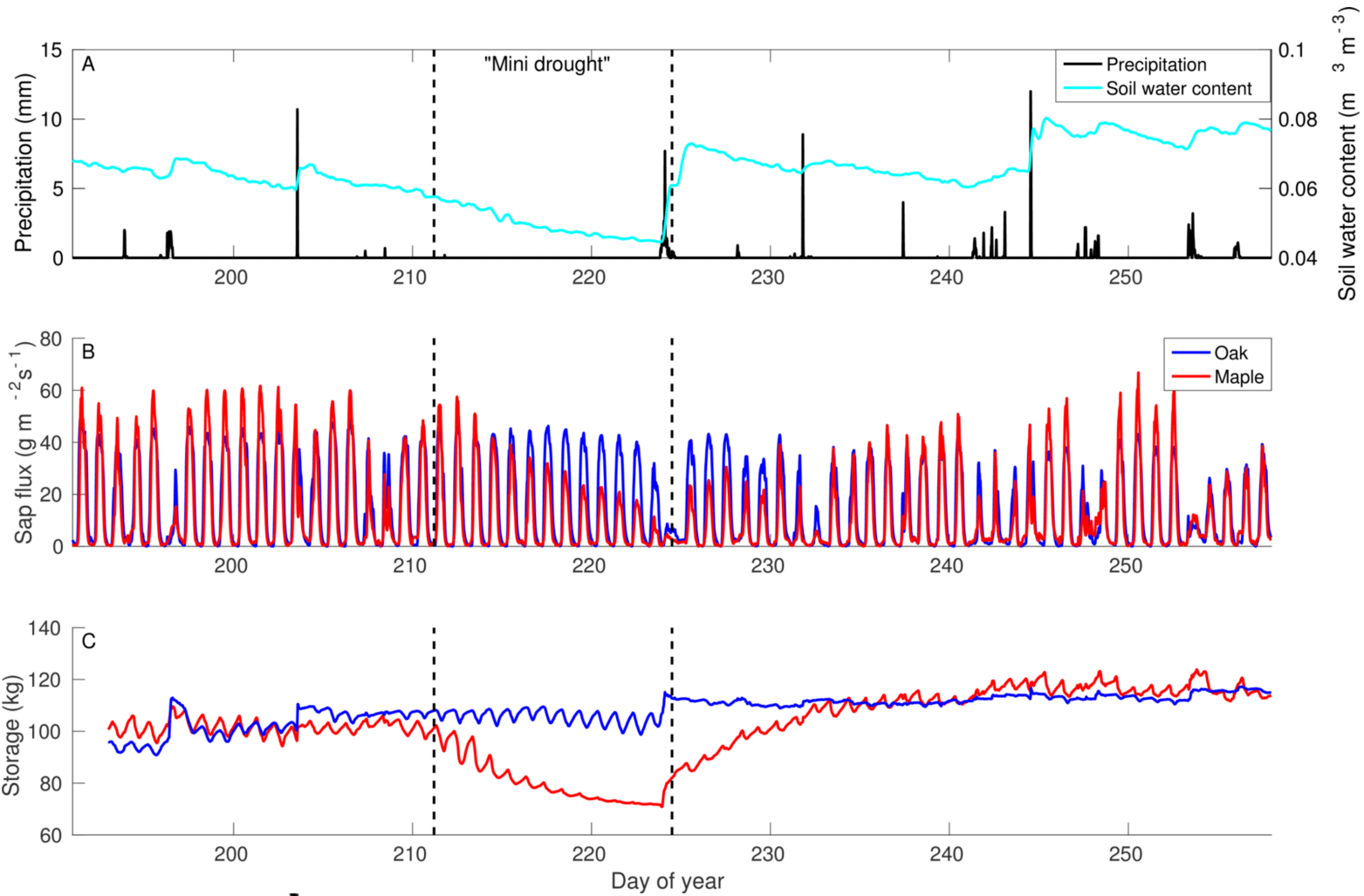
pt



Al

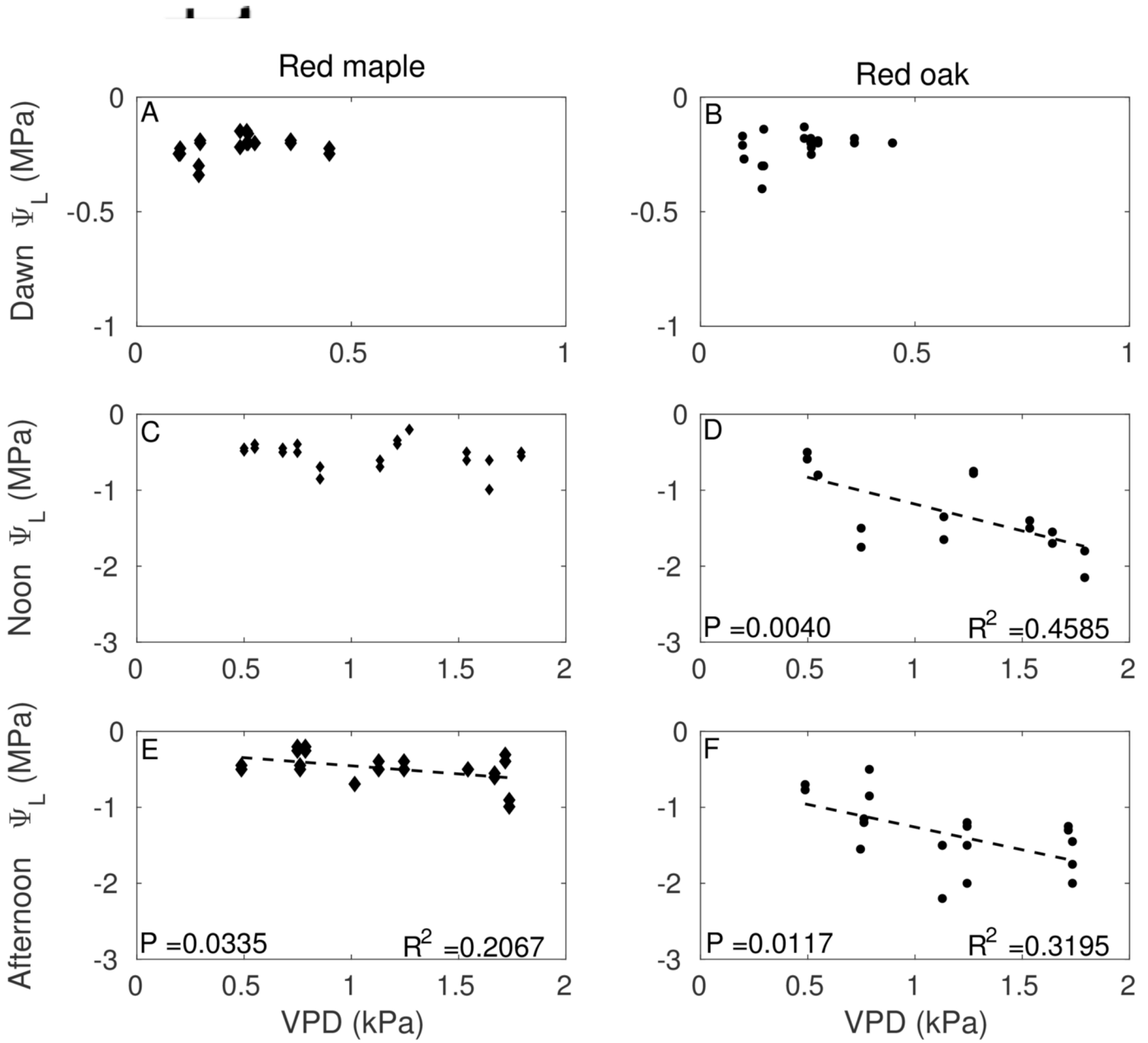
eco_1815_f2.eps

pt

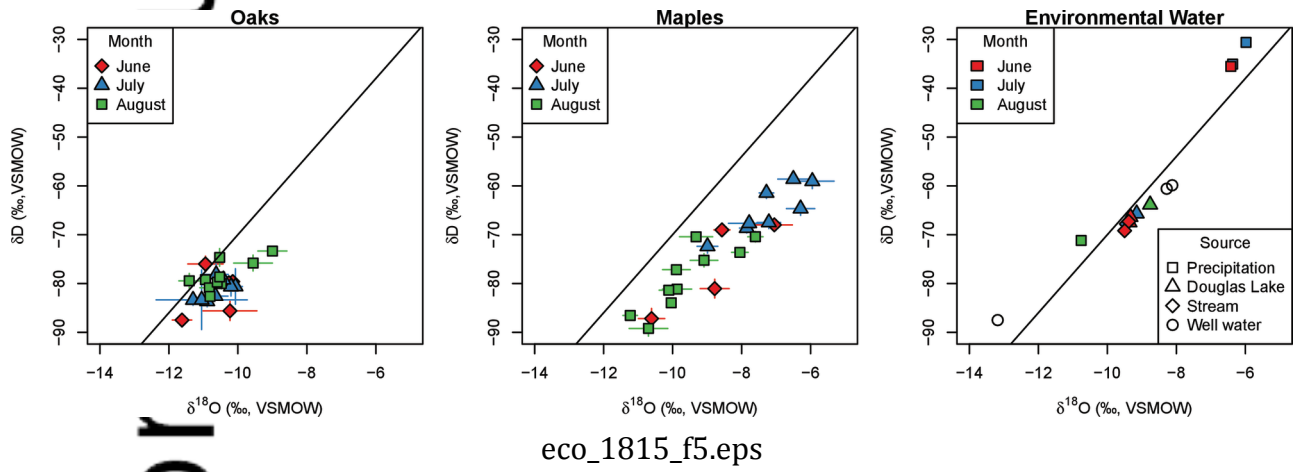


eco_1815_f3.eps

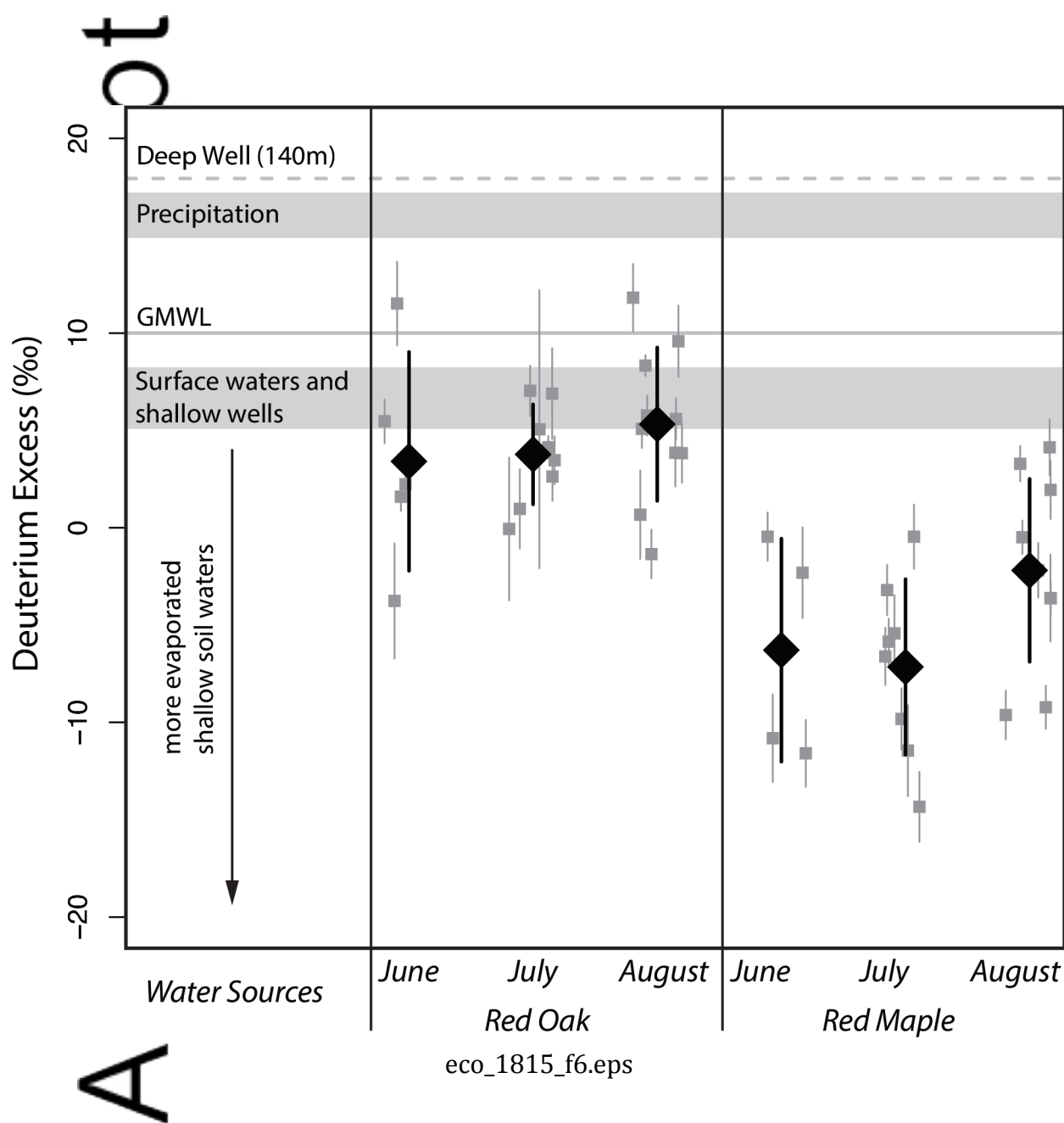
AL

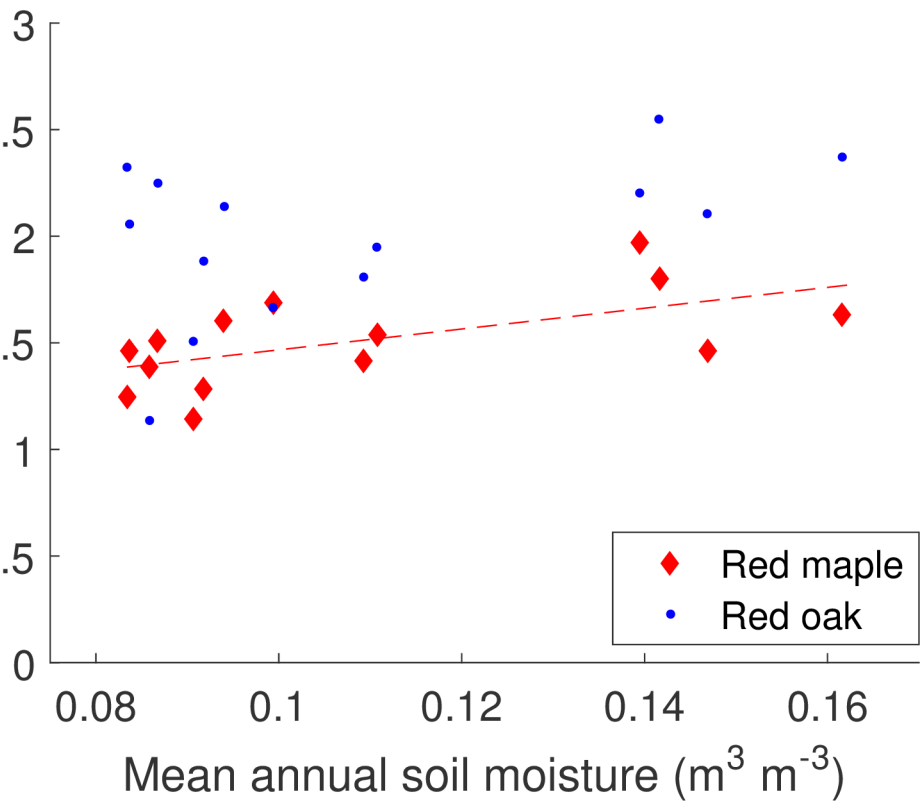


eco_1815_f4.eps



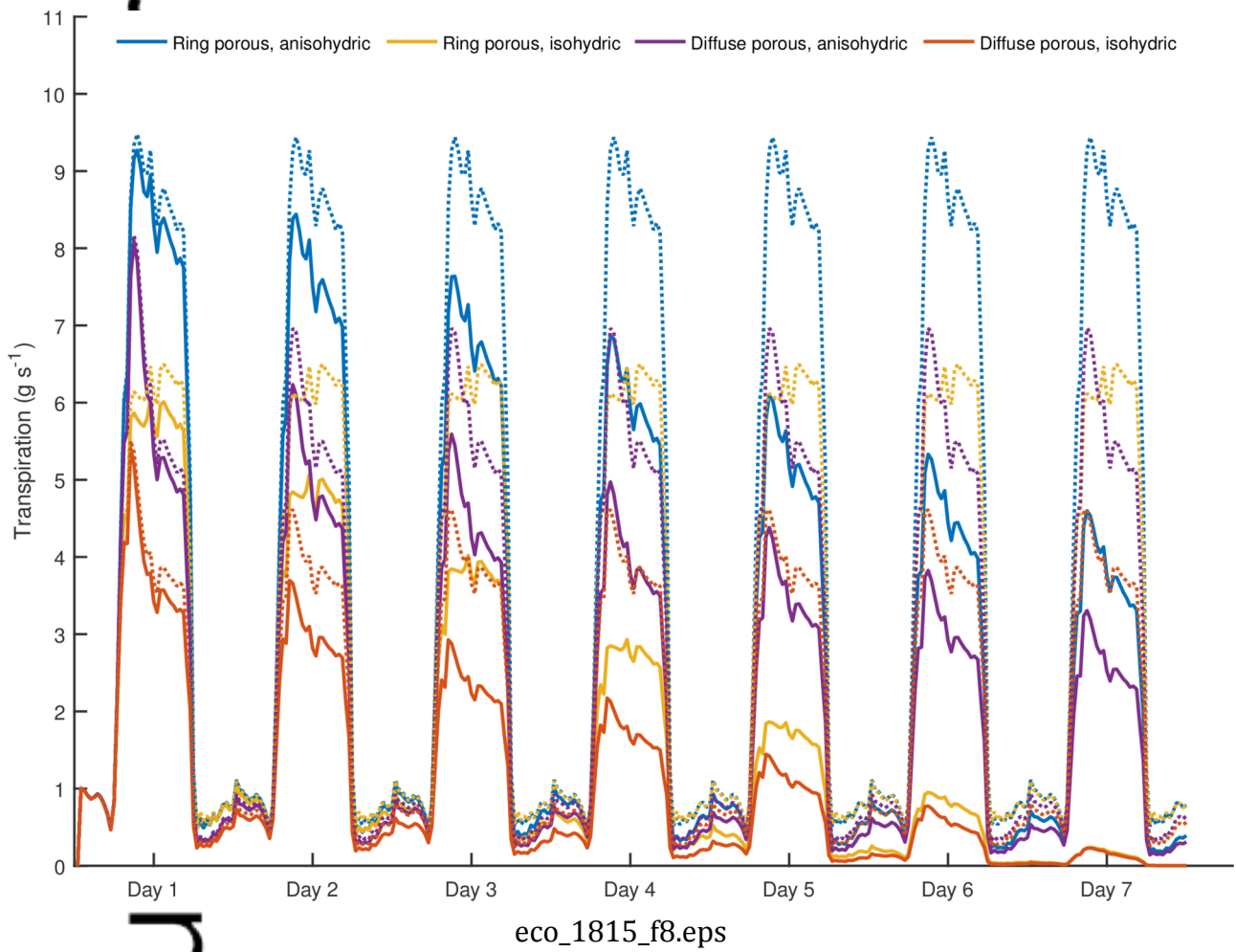
eco_1815_f5.eps





eco_1815_f7.eps

ipt



Au